Science of the Total Environment 912 (2024) 169246

Contents lists available at ScienceDirect

Science of the Total Environment

journal homepage: www.elsevier.com/locate/scitotenv

# Effects of global and climate change on the freshwater-seawater interface movement in a Mediterranean karst aquifer of Mallorca Island

Diana Puigserver [a], Jordi Giménez [b,c], Francesc Gràcia [c,d], Àlvaro Granell [c,d], José M. Carmona [e,*], Aina Torrandell [e], Joan J. Fornós [c,d]

[a] Department of Mineralogy, Petrology and Applied Geology, Faculty of Earth Sciences, University of Barcelona (UB), Water Research Institute (IdRA-UB), Serra Húnter Tenure-elegible Lecturer, C/ Martí i Franquès, s/n, E-08028 Barcelona, Spain
[b] General Directorate of Water Resources of the Balearic Islands, C/ Gremi Corredors, 10, E-07009 Palma, Mallorca, Spain
[c] Earth Sciences Research Group, Department of Biology, Universitat de les Illes Balears, Cra. Valldemossa, km 7.5, E-07122 Palma, Mallorca, Spain
[d] Societat Espeleològica Balear, C/. Margarida Xirgu, 16, E-07011 Palma, Mallorca, Spain
[e] Department of Mineralogy, Petrology and Applied Geology, Faculty of Earth Sciences, University of Barcelona (UB), Water Research Institute (IdRA-UB), C/ Martí i Franquès, s/n, E-08028 Barcelona, Spain

## HIGHLIGHTS

- In double-flow karst aquifers, flow in conduits may supply solutes to the rock-matrix.
- Irrigation returns, re-evaporated and saline waters, increase aquifer salinization.
- Aquifer salinization sodifies agricultural soil.
- Soil sodification is an adverse effect of climate change-driven drought.

## GRAPHICAL ABSTRACT

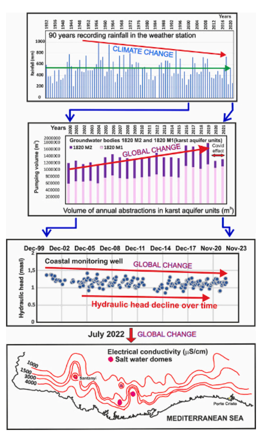


## ARTICLE INFO

Editor: José Virgílio Cruz

*Keywords:*
Boron isotope composition
Double flow and triple flow
Rebound effect
Recycled evaporated waters
Seawater intrusion in karst aquifers
Strontium isotope ratio

## ABSTRACT

Karst aquifers are globally prized freshwater sources, posing a significant preservation challenge. These aquifers typically exhibit dual or even triple porosities, encompassing matrix, fractures-fissures and conduits, rendering them highly responsive to variations in chemical characteristics and hydraulic head. In coastal regions, these aquifers often possess extensive subsurface conduit networks intricately linked to the rock matrix, facilitating groundwater discharge into the sea. Therefore, they display acute sensitivity to seawater intrusion, swiftly reacting to changes in precipitation and pumping regimes. This makes them exceptionally vulnerable to short-term meteorological fluctuations and long-term climate change. Their high heterogeneity leads to uneven penetration of the freshwater-seawater interface, causing rapid seawater intrusion inland over significant

* Corresponding author.
*E-mail address:* jmcarmona@ub.edu (J.M. Carmona).

https://doi.org/10.1016/j.scitotenv.2023.169246
Received 28 June 2023; Received in revised form 30 November 2023; Accepted 7 December 2023
Available online 9 December 2023

distances. The Mediterranean region, characterized by water deficit and water stress, faces strong impacts from climate change, featuring a warming atmospheric trend exceeding the global average, along with diminished rainfall exacerbating water scarcity. Increasing water demands for agriculture, urban development, and the growing tourism industry, because of global change, are worsening water stress. Our primary research objectives were analyzing the environmental consequences of global and climate change on seawater intrusion in Mediterranean coastal karst aquifers, with a focus on the role of the double-flow model, thus contributing to the understanding of the processes involved. To achieve this, we selected a study region on Mallorca Island in the western Mediterranean, where a karst aquifer system discharges into the sea. We employed various study methods, notably hydrochemical techniques and multi-isotopic analysis, encompassing the examination of $^{2}$H and $^{18}$O isotopes in water, $^{87}$Sr/$^{86}$Sr ratio, Sr and B concentrations, and $\delta^{11}$B in water. A key finding is the rebound effect, wherein aquifers recontaminate due to solute molecular back-diffusion following cessation of extractions and the retreat of marine intrusion, providing insight into the impact of climate and global change on Mediterranean karst aquifers.

## 1. Introduction

Carbonate karst aquifers are among the most valued as a source of freshwater for drinking water supply (Ford and Williams, 2007; Kalhor et al., 2019). It has been estimated that 10 % of the world population is supplied by these aquifers (Stevanović, 2019), although other authors have provided values of up to 25 % (Smart and Worthington (2004). Considering that 15.2 % of the outcropping carbonate rocks are karstifiable (Goldscheider et al., 2020), their preservation as a water resource represents a crucial challenge. These hydrosystems are very heterogeneous and vulnerable to contamination because they are connected to the ground surface (Kalhor et al., 2019; Masciopinto et al., 2021; Marín et al., 2021), and in the case of coastal aquifers subject to significant groundwater abstraction, they are also vulnerable to seawater intrusion because they are in contact with the sea (De Filippis et al., 2020).

These aquifers are characterized by three types of porosity (Yadav et al., 2022): i) intergranular matrix porosity (primary porosity), ii) fracture or fissure porosity (secondary porosity), and iii) karst conduits (tertiary porosity). These porosity types lead to a heterogeneous distribution of the hydraulic conductivity of the aquifer and, accordingly, of groundwater flow (Mohammadi et al., 2021). These systems are known to have double (dual), and even triple, porosity; or in other words, they are double (dual) flow systems through the matrix and karst conduits (Reimann et al., 2011; Zhao et al., 2022). The matrix, which is characterized by large storage volumes of groundwater (Yadav et al., 2022), consists of primary porosity sensu stricto and/or fractured rock (secondary porosity due to fracturing or fissuring). Throughout this matrix, there is a laminar flow governed by the Darcy law (Masciopinto et al., 2021) when the matrix is equivalent to what would correspond to a granular type medium, or by the cubic law when it corresponds to a fractured medium (Ford and Williams, 2007).

In contrast, flow through karst conduits (tertiary porosity) is usually turbulent (Wu and Hunkeler, 2017) and can be described, among other approximations, by the Darcy-Weissbach (Brown, 2003; Li et al., 2022) or Poiseuille (Wang, 2010) equations or, in the case of the circulation in cavities, by the Manning equation (White, 2016). Turbulent flow tends to be prevalent and largely controls the transport of ions and other substances in solution in groundwater in karst conduits (Ghasemizadeh et al., 2012).

Water exchange between the matrix and karst conduits can be variable and has been the subject of numerous studies (as reported by Martin et al., 2006; Bailly-Comte et al., 2010; Reimann et al., 2011; Binet et al., 2017; Sivelle et al., 2019). This exchange is not only quantitatively important, but is also relevant to understand solute transport in these karst aquifers (Chang et al., 2019; Kresic and Panday, 2021). Thus, during periods when the water table levels within the three-dimensional conduit network are higher than the top of the conduits, groundwater flows from the conduits to the host rock matrix when hydraulic gradients are directed from the conduits to the rock matrix. This could lead to the penetration of contaminants into the matrix if the conduit is contaminated. Conversely, when hydraulic gradients are directed from the host rock towards the conduit network, the opposite situation may occur. Additionally, in periods when hydraulic heads fall below the top of conduits, the matrix could introduce contaminants into these karst conduits (Ghasemizadeh et al., 2012; Martin et al., 2012; White et al., 2016).

The comprehensive data analysis of hydraulic heads, hydraulic parameters (obtained from pumping tests), groundwater hydrochemic and isotopic parameters (Barbieri et al., 2005; Calligaris et al., 2018), together with geological data, constitute useful tools for the establishment of conceptual models of double porosity flow in karst aquifers (Goldscheider, 2015). Traditionally, the oxygen and hydrogen isotopic composition of the water molecule ($\delta^{18}$O and $\delta^{2}$H) has been used as a tracer to understand the hydrodynamics of aquifers, allowing to characterize, among other aspects, the recharge zone (Clark and Fritz, 1997; Chou et al., 2022) and water mixing processes (Clark and Fritz, 1997; Behera et al., 2019; Li et al., 2019).

Simplified flow models include the piston-flow model (PFM), exponential-mixing model (EMM), and dispersion model (DM) (Maloszewski and Zuber, 1996; De Waele and Gutiérrez, 2022). In karst systems where conduit flow predominates, the isotopic composition of groundwater tends to be homogeneous, preserving the average isotopic fingerprint of the recharge zone if the altitude of this zone is similar, which agrees with a PFM-type flow model (Bicalho et al., 2019). On the contrary, in those karst aquifers where there is exchange between the matrix and the karst conduits, the isotopic composition of groundwater is heterogeneous, following an EMM model. However, flow in karst aquifers is often described as a combination of EMM and PFM models (Brkić et al., 2018).

The double-flow makes karst aquifers highly dynamic and sensitive to variations in their chemical characteristics and hydraulic head. These aquifers offer a rapid response to rainfall and pumping, which makes them very vulnerable to short-term weather variations and long-term changes in climate (Long and Mahler, 2013). Karst aquifers in coastal areas with double-flow often have extensive and well-developed subsurface networks of conduits that discharge groundwater to the sea (Beddows et al., 2007; Ford and Williams, 2007), making these aquifers very sensitive to seawater intrusion (Han et al., 2015; Biondić et al., 2022).

The high heterogeneity of these aquifers favors uneven penetration of the seawater intrusion, with a mixing zone moving vertically and laterally (Calvache and Pulido Bosch, 1997; Dokou and Karatzas, 2012; Xu et al., 2016, 2019), which facilitates the rapid penetration of seawater many kilometers inland (Werner et al., 2013). In addition, the double porosity may foster interface penetration into the matrix (Xu et al., 2018), which explains why the intrusion can persist for decades.

The effect of climate change on the recharge pattern also has an effect on the penetration of the marine wedge into karst aquifers (Romanazzi et al., 2015). In arid or semi-arid climates, decreased recharge reduces the discharge rate to the sea, leading to increased seawater penetration (Green and MacQuarrie, 2014; Costall et al., 2020).

Furthermore, small rises in sea level can potentially move the freshwater-seawater interface inland (Shi et al., 2020; Zhang et al., 2022b), potentially penetrating kilometers in the case of karst conduits (Vera et al., 2012; Menning et al., 2015; Guo et al., 2020).

Inland seawater penetration is strongly controlled by the abstraction regime in the aquifer (Custodio, 2012; Ferguson and Gleeson, 2012; Purnama and Marfai, 2012; Motevalli et al., 2018; Wu et al., 2022). This penetration is known as seawater intrusion and is especially significant in coastal regions where important tourist and industrial areas are concentrated such as those studied by Aureli et al. (2006). In the case of karst aquifers, the fact that wells abstracting the highest flow rates are located in the hydraulically most conductive zones (Bakalowicz, 2005; Wang et al., 2021), favors a rapid rise of the freshwater-seawater interface and the consequent formation of salt-water domes (Etsias et al., 2021).

To determine the position and mobility of the freshwater-seawater interface, numerous geological (Zamrsky et al., 2020), hydrodynamic (Vallejos et al., 2015); and geophysical (Duque et al., 2008) techniques have traditionally been used. More recently, hydrogeochemical and isotopic tools are among the most widely used (Lim et al., 2013; Vallejos et al., 2015; Bagheri et al., 2019; Nair et al., 2021). Moreover, increasingly, multi-isotopic analysis of $\delta^2$H, $\delta^{18}$O, $\delta^{11}$B, and $^{87}$Sr/$^{86}$Sr has been incorporated into the seawater intrusion characterization studies (Cary et al., 2015; Brenot et al., 2015).

The freshwater-seawater interface consists of a transition zone in which fresh waters from the aquifer mix with those from the sea. These mixing waters have a certain isotopic composition in $^2$H and $^{18}$O according to the different mixing ratios. The original proportion of aquifer and sea water in the transition zone can be known from the original $\delta^2$H or $\delta^{18}$O values of each water, since the waters of this zone align along a straight mixing line (Mook, 2002; Capaccioni et al., 2005; Mongelli et al., 2013). Additionally, the use of boron and strontium isotopes allows to identify both hydrochemical processes occurring because of water-rock interaction, and processes resulting from the mixing of freshwater with seawater (Jørgensen et al., 2008; Langman and Ellis, 2010; Werner et al., 2013; Mahlknecht et al., 2017). Sr concentrations and the $^{87}$Sr/$^{86}$Sr isotope ratios are also used to determine hydrochemical water-rock interaction processes and to identify groundwater sources of different origins (Frost and Toner, 2004; Ribeiro et al., 2014; Brenot et al., 2015; Zhang et al., 2022a). These isotopes are also used to characterize groundwater mixing and flow paths in the upper and deeper parts of karst aquifers, making them good tracers (Wang et al., 2006).

To study the origin of groundwater and the kinetics of hydrochemical reactions involving dissolved boron species in these waters, $\delta^{11}$B values are also of great utility (Cary et al., 2015; He et al., 2018; Stefánsson et al., 2019). Present-day seawater exhibits stable values in $\delta^{11}$B of 39.5 ‰ in average (Spivack and Edmond, 1987; Mao et al., 2020) and in $^{87}$Sr/$^{86}$Sr of 0.7092 (Jørgensen et al., 2008; Mao et al., 2020). Therefore, the $\delta^{11}$B - $^{87}$Sr/$^{86}$Sr pair can be used as a tracer to identify water sources (Mao et al., 2020). In general, it is observed that Boron concentrations are generally higher in freshwaters than in marine waters, so the trend of decreasing B concentrations in groundwater of coastal karst aquifers is indicative of salinization by seawater intrusion (Russak et al., 2016). In contrast, Sr concentrations are high in marine waters and low in groundwater (Mahlknecht et al., 2017). In addition, seawater exhibits more positive $\delta^{11}$B values and a lower $^{87}$Sr/$^{86}$Sr ratio than groundwater (Mao et al., 2020).

The Mediterranean region, characterized by scarce precipitation and water stress, is being strongly affected by climate change (Lukač Reberski et al., 2020), showing a warming trend higher than the global average. Temperatures are predicted to increase by 2.2 °C by 2040 compared to pre-industrial times, while increased evapotranspiration and reduced rainfall could decrease water availability by 2–15 % (Cramer et al., 2018). This trend, together with the increasing water demand for agricultural and urban development, as well as the growing tourism industry, is worsening water stress in the region and will increase further in the near future. In addition, the total population of this region is expected to increase by 90 million people in the next 30 years, reaching 611 million in 2050 (Ambrosetti, 2020). Droughts and human activity developed especially in the second half of the 20th century, a period that included the most extreme drought events of the last century, especially in the Mediterranean region (Nicault et al., 2008; Cinkus et al., 2023) have led to the quantitative and qualitative decline of water resources in the region. This, together with the sustained sea level rise due to global warming (Abd-Elhamid and Javadi, 2011; Ketabchi et al., 2016), could have devastating effects on water resources and thus on natural terrestrial and marine ecosystems, agriculture, recreation, tourism, and human health.

When two types of groundwater with different ionic strength and nearly saturated in calcite are mixed, the resulting solution is undersaturated with respect to this mineral, as reported by Back et al. (1979). This effect occurs, for example, in the coastal zone of karst aquifers in the case of the freshwater-saltwater interface. However, although this is true, studies conducted by Gulley et al. (2015) have argued that the main driving force behind coastal mixing solution is $CO_2$.

In the Mediterranean region, numerous coastal karst aquifers exist (Aureli et al., 2008). Their karst conduits discharge into the sea. In addition, numerous caves, associated with sea level oscillations, have developed (Antonioli et al., 2021). These endokarst structures favor the penetration velocity of the seawater intrusion, especially in areas where intense abstraction is occurring (Döll, 2002; Aureli et al., 2008). The decrease in aquifer recharge and sea level rise, due to climate change and global warming, will encourage salinization processes in Mediterranean coastal aquifers (Wöppelmann and Marcos, 2012; Feng et al., 2013).

The primary aim of this study is to assess the impact of global and climate change scenarios on seawater intrusion in a coastal karst aquifer in Mallorca, while considering the broader implications for Mediterranean coastal areas. Additionally, we seek to enhance our understanding of the underlying processes and analyze the relevance of the double-flow model in explaining seawater intrusion.

Two working hypotheses were proposed in this study:

First working hypothesis: The double-flow in coastal karst aquifers is an additional factor contributing to the deterioration of groundwater quality as the freshwater-seawater interface advances inland during extended drought periods or when extractions increase.

Second working hypothesis: Although during periods of significant recharge seawater intrusion recedes following extreme rainfall events or during the cessation of extractions, back-diffusion of chloride and other solutes from the smaller pores in the host rock matrix, contaminate once again the aquifer (rebound effect).

## 2. Hydrogeological framework of the Serres de Llevant-Marina de Llevant aquifer system

To demonstrate the validity of the working hypotheses, a study region was chosen on Mallorca Island, in the western part of the Mediterranean Sea and off the eastern coast of the Iberian Peninsula (Fig. 1A). Specifically, this region includes a part of the Serres de Llevant range and the Marina de Llevant (Fig. 1A). Climate in the region is typically Mediterranean, with hot, dry summers and mild, humid winters. The average annual rainfall ranges between 300 and 500 mm, and the average annual temperatures vary between 16 and 17 °C, although on occasion it can reach 41 °C during the summer and 6 °C in winter (Ginés et al., 2012). Rainfall events are infrequent but intense, and approximately 70 % of the annual rainfall occurs in less than 20 days.

From a hydrological point of view, the study region constitutes the Serres de Llevant-Marina de Llevant aquifer system (López-García and Mateos Ruiz, 2003). This is an intensely karstified carbonate aquifer system (Giménez et al., 2014), Fig. 1A.

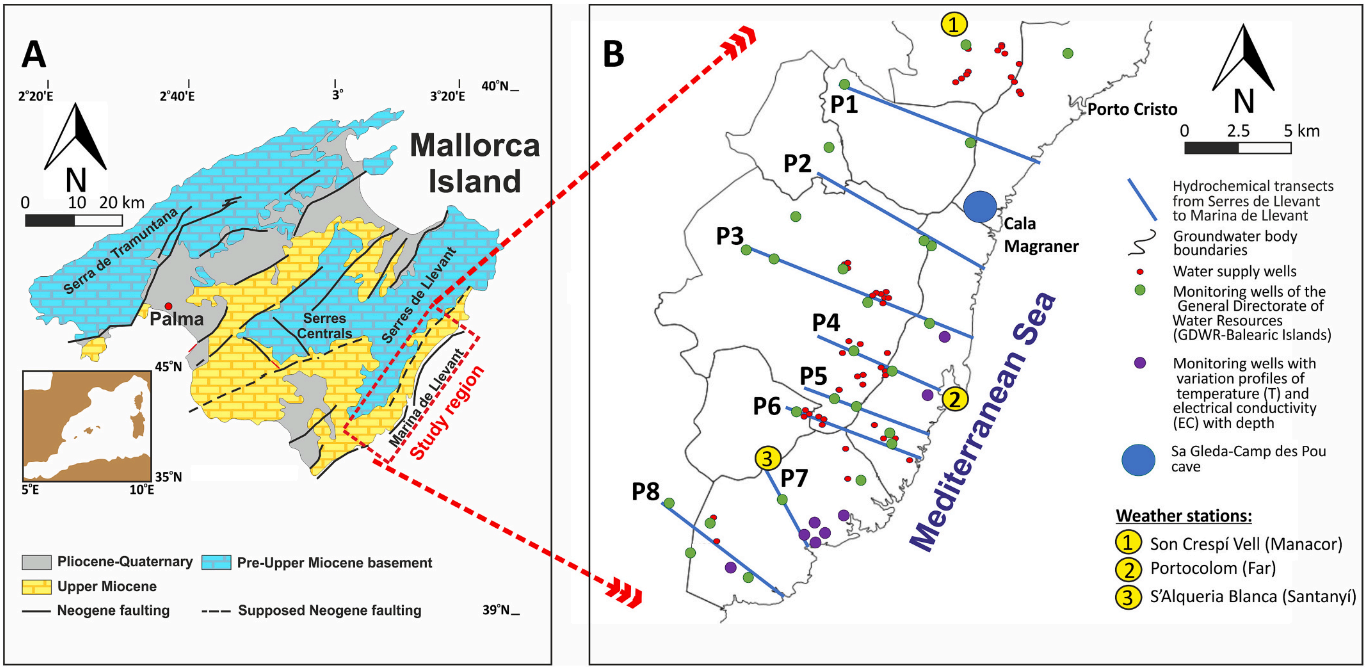


**Fig. 1.** (A) Location map of the study region within the context of Mallorca Island in the western Mediterranean. (B) Network of groundwater quality monitoring wells (water supply wells) and hydraulic head monitoring of the General Directorate of Water Resources of the Balearic Islands (GDWR-BI). Monitoring wells in which profiles of Temperature (T) and Electrical Conductivity (EC) variation with depth were carried out are highlighted. Transects P1 to P8 made up of hydrochemical monitoring wells from the Serres de Llevant range to the Marina de Llevant and up to the coastline are also shown.

The aquifer system in the Serres de Llevant range is predominantly formed by unconfined carbonate aquifers consisting of Liassic and Upper Triassic dolostones and limestones. In the Marina de Llevant, the aquifer layers are formed by Miocene bioclastic calcarenites and Jurassic dolostones (Fornós and Gelabert, 2011). In general, the Miocene rocks and the upper levels of Jurassic dolostones are hydraulically connected and show a very high karstification degree, as evidenced by the karstic caves distributed along the coastline (Gràcia et al., 2011). The aquifer

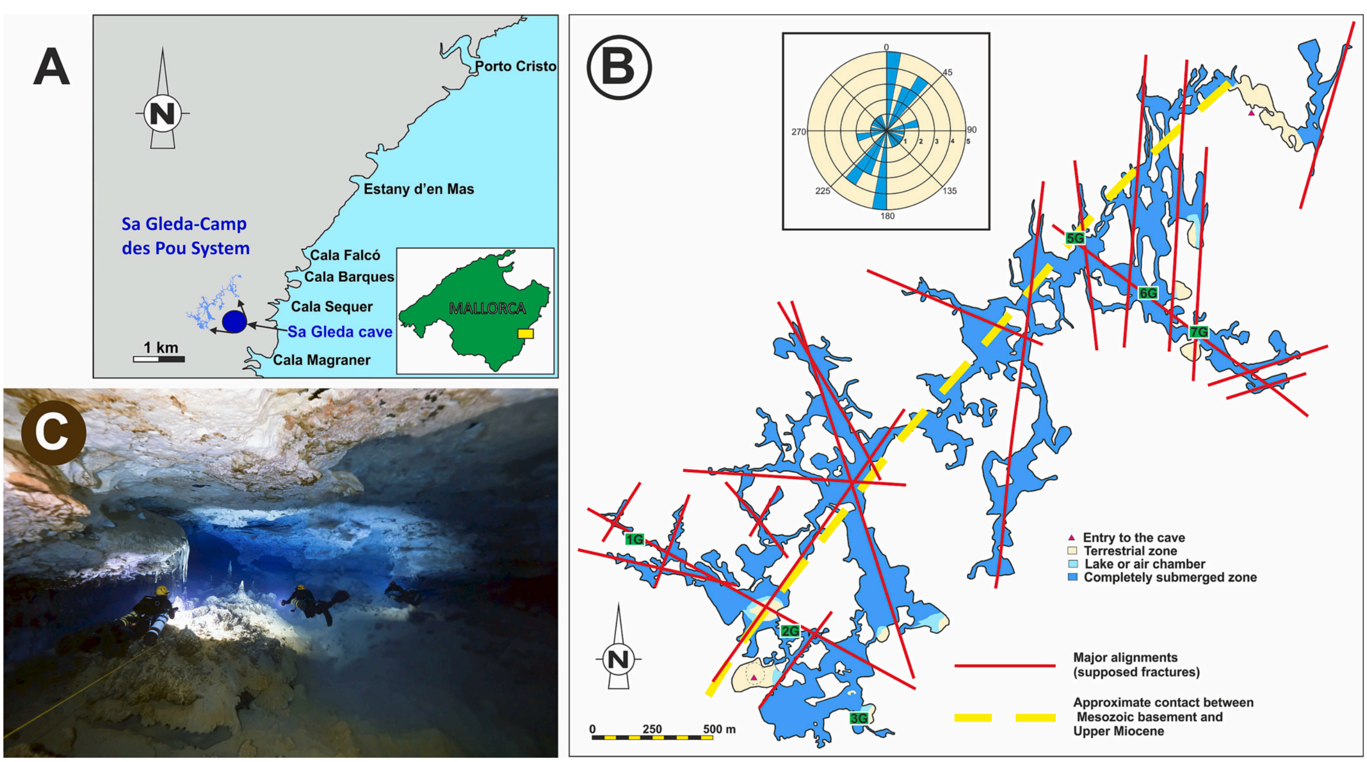


**Fig. 2.** (A) Location of the underwater Sa Gleda-Camp des Pou cave. (B) Topography of the cave (adapted from Fornós and Gràcia, 2021) with location of the depth sampling profiles 1G, 2G, 3G, 5G, 6G and 7G (Table 2), as well as the rose diagram plot of fractures in the cave. (C) Detailed photograph of topographic mapping and fracture measurement operations (Fornós and Gràcia, 2021).

system is fractured, forming a network whose main fracturing directions are NW-SE, on which dry streams are placed, and NE-SW, parallel to the coastline. The natural discharge of the aquifer system into the sea occurs in the coastal area of the Marina de Llevant and takes place through the karst conduit network developed following the fracture network and its connection with the aforementioned caves of the coastline.

From the group of caves distributed throughout the studied region, the Sa Gleda-Camp des Pou cave has been selected because of its size and importance (Figs. 1B, 2A, 3F). It is a karst cave developed in the Marina de Llevant Miocene carbonate platform (Gràcia et al., 2010) and presents different galleries, chambers and conduits (Fig. 2B,C) that, according to Fornós and Gràcia (2021), are arranged more or less perpendicular to the predominant NW-SE direction. On the basis of the topography of the cave provided to date by these authors, the cave has an approximate development of about 14,620 m, of which 13,720 m are sub-aquatic and 900 m are aerial. In Fornós and Gràcia (2021) a detailed description of the lithological units in which the cave is carved is given.

The monitoring network of the study region (Fig. 1B) is managed by the General Directorate of Water Resources of the Balearic Islands (GDWR-BI). This is a double network; on the one hand, it is composed of private and public supply wells. Although the most common monitoring frequency is monthly, there are also bimonthly, quarterly, and annual frequency of monitoring of water quality. On the other hand, the monitoring of hydraulic heads is carried out with a piezometer network that provides monthly hydraulic head measurements.

The Serres de Llevant-Marina de Llevant aquifer system is characterized by two well-differentiated lithostratigraphic series, as described in detail by Fornós and Gelabert (2011). Fig. 3A shows the type lithostratigraphic series that constitute the geological framework of this aquifer system.

The characteristic type series of the Serres de Llevant range (Fig. 3A) is made up of carbonate Mesozoic rocks. The substrate of the aquifer system coincides with the detachment levels represented by pelitic sediments with red and yellowish marls and with evaporitic layers typical of the Keuper facies (Upper Triassic). Above these detachment materials, there are Supra-Keuper (Triassic) or Infra-Lias dolostones hydraulically connected with limestones and strongly brecciated dolostones of the Lias (Lower Jurassic). The group of these hydraulically connected materials constitutes an unconfined (Fig. 3A) heavily exploited hydrogeological complex in the Serres de Llevant range (laterally connected with the lower part of another aquifer in the Marina de Llevant, see below). Transmissivity in the hydrogeological complex is high, varying between 200 and 700 $m^2$/day, although there are zones in the Serres de Llevant range with values of up to 1400 $m^2$/day (evidence of karstification of this hydrogeological complex was described by Fornós and Gelabert, 2011). The Supporting information document (SI document) provides data of hydraulic parameter values obtained by pumping tests in the study region.

The Middle to Upper Jurassic materials are composed of alternating limestones and marls, thus constituting a multilayered hydrogeological complex (materials not shown in the type lithostratigraphic series Fig. 3A). Overlaying this complex, there are Cretaceous materials dominated by marls acting as an aquitard (not shown in Fig. 3A). Between the Cretaceous and Eocene materials, there is a hiatus. Oligocene materials (not shown in Fig. 3A) formed by calcarenites and marls with interstratified levels of sandstones and conglomerates are found overlaying the hiatus (Fornós and Gelabert, 2011). The Lower and Middle Miocene (turbidites and calcarenites) have little continuity in the Serres de Llevant range and are of no hydrogeological interest (not shown in Fig. 3A).

In the Marina de Llevant two important hydrogeological complexes exist (Fig. 3A). The first complex (lower hydrogeological complex) is formed by the Mesozoic basement materials (essentially made up of the Supra-Keuper or Infra-Lias dolostones and the most brecciated levels).

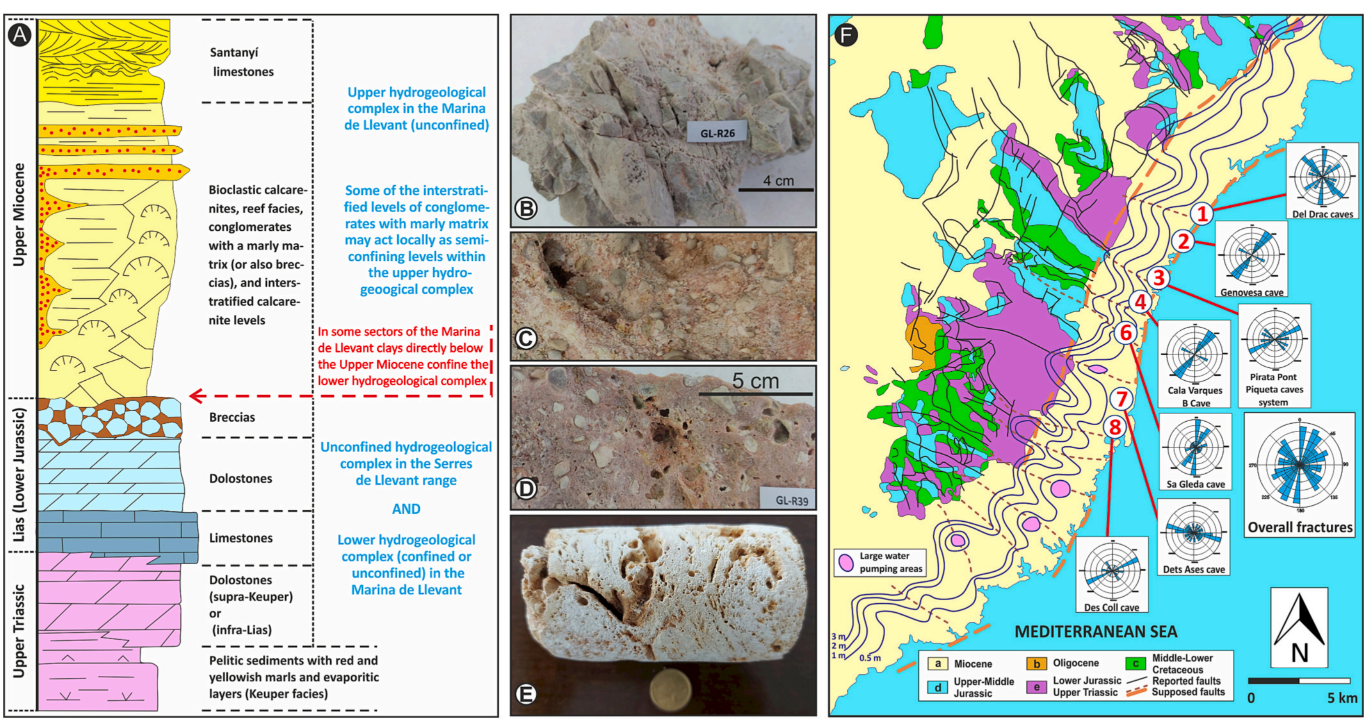


**Fig. 3.** (A) Type lithostratigraphic series of the Serres de Llevant range and Marina de Llevant (adapted from Moragues et al., 2021; Fornós and Gràcia, 2021). (B) to (E) Photographs of rock hand samples from the studied region showing different details related to porosity (Fornós and Gràcia, 2021): (B) Tectonized dolostone of the Mesozoic basement, (C) conglomerates and microconglomerates of the Upper Miocene mostly supported by sandy matrix, (D) Section view of the sample in the previous photograph, (E) Core sample of the Santanyí bioclastic limestones. (F) Hydraulic head map of the Serres de Llevant-Marina de Llevant aquifer system (July 2022), and geological map with the main outcropping materials and fractures. Geological legend: (a) Miocene (limestones and marls of reef facies, oolitic-stromatolitic limestones, silts, sandstones and conglomerates); (b) Oligocene (marls and limestones); (c) Middle-Lower Cretaceous (marls and marlstones); (d) Upper-Middle Jurassic (marls, marlstones and detritic limestones); (e) Lower Jurassic-Upper Triassic (marls and dolostones).

The second complex (upper hydrogeological complex) is formed by the Upper Miocene materials (principally constituted of bioclastic calcarenites and limestones). The dolostones of the first hydrogeological complex have high transmissivities (between 200 and 850 $m^2$/day) and lateral hydraulic connection with the unconfined hydrogeological complex of the Serra de Llevant range, as mentioned above. The lower hydrogeological complex of the Marina de Llevant is confined in some sectors by ochre and reddish clays with some cobbles. These materials act as an aquitard, and their thickness is variable, ranging between 14.5 and 15.5 m. Above this aquitard, where it exists, there is the upper hydrogeological complex. When the aquitard is lacking, the Upper Miocene materials of the upper hydrogeological complex overlie directly the lower hydrogeological complex. The base of the Upper Miocene consists of bioclastic calcarenites, reef facies, conglomerates with a marly matrix (or also breccias), and interstratified calcarenite levels. Some of the interstratified levels of conglomerates with marly matrix may act locally as semiconfining levels within the upper hydrogeological complex. The Miocene sequence culminates with the Santanyí limestones (Fornós and Gelabert, 2011).

In the coastline area of the Marina de Levant, where the Sa Gleda-Camp des Pou cave is located, it has been observed that the Mesozoic materials of the lower hydrogeological complex and those at the base of the Upper Miocene unit (bioclastic calcarenites) of the upper hydrogeological complex are laterally connected and have high transmissivities caused by the high primary effective porosities (ranging from 0.5 to 18 %, see the SI document) and high degree of karstification. This is also evidenced by the development of both exokarstic and endokarstic forms (Fornós et al., 2019; Ginés et al., 2021). Among these endokarstic forms, underwater caves located along the coastline stand out (Figs. 2, 3F and 4, Gràcia et al., 2010, 2011). These are cavities where there is a zone at a determined depth in which fresh groundwater mixes with brackish and marine waters.

## 3. Materials and methods

### 3.1. Meteorological and groundwater abstractions data

To analyze the effect of climate change on the water resources of the aquifer system, historical rainfall data from the weather stations network of the State Meteorological Agency of Spain (*Agencia Española*

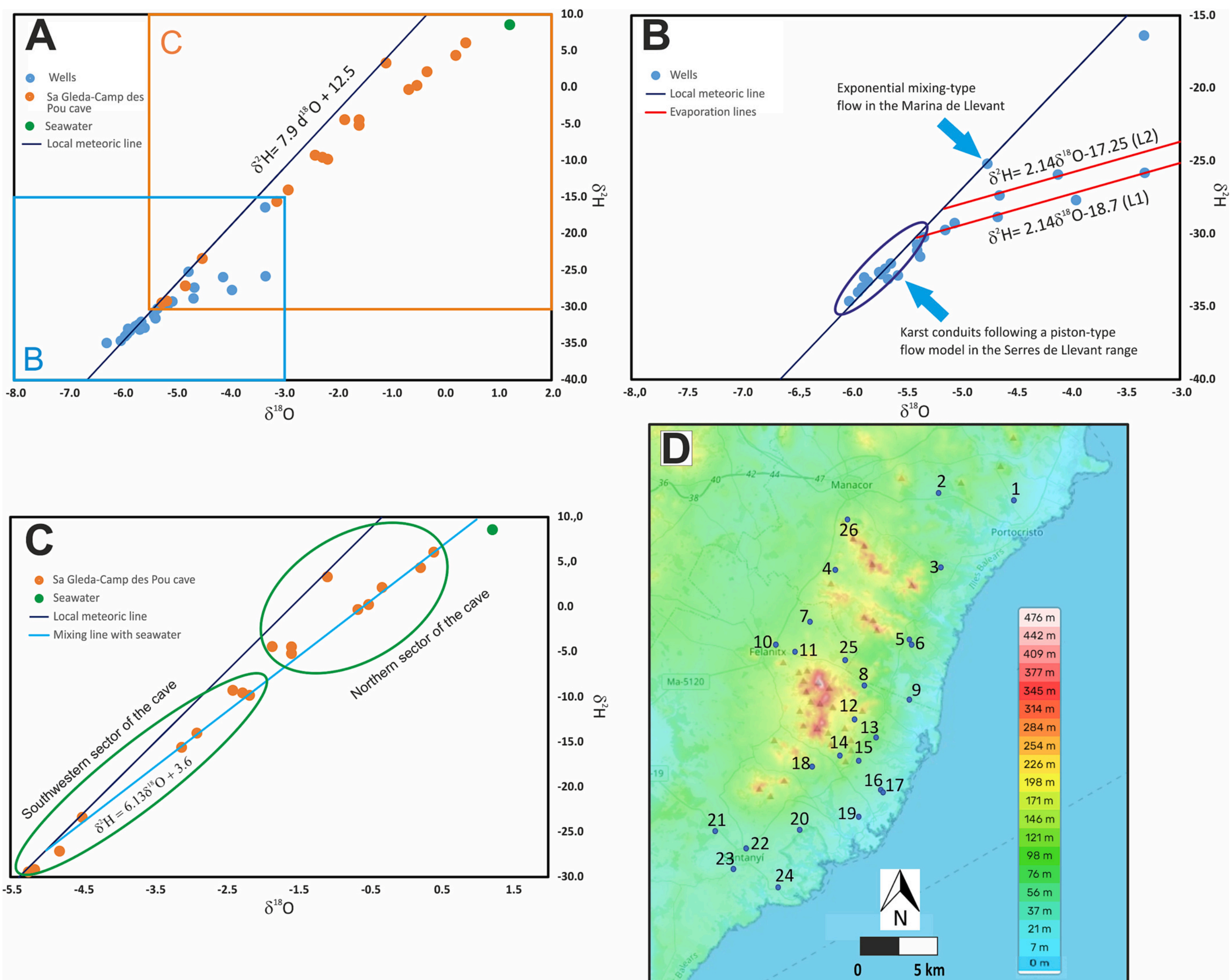


**Fig. 4.** (A) $^{18}$O and $^{2}$H plot where water samples from the monitoring wells and Sa Gleda-Camp des Pou waters sampled in July 2022 are represented (VSMOW standard). (B) Detailed view of the groundwater samples from the wells (local meteoric water line and evaporation lines of groundwater used in agriculture affected by saltwater intrusion and successive cycles of recycling of irrigation returns). (C) Detailed view of the water samples from the cave. (D) Location of the water samples from the wells in relation to the topography of the area (altitudes at a distance of 5 km and the coastline correspond to the Marina de Llevant, Fig. 3F).

*de Meteorología*, AEMET) in Mallorca were collected. Specifically, the series of historical annual precipitation data obtained from the monthly values of the last 90 years for three localities in the study region were analyzed (Manacor-Son Crespí Vell, Felanitx-Far de Portocolom, and Santanyí-S'Alqueria Blanca, see Fig. 1B). The impact of climate change on the decrease in hydraulic heads was thus evaluated. Table SI–1 of the SI document provides data of the periods for which rainfall records are available, as well as the UTM coordinates, and the station altitude (masl).

The impact of global change on hydraulic heads was assessed by studying the evolution of groundwater abstractions for drinking water supply. The analysis of the relationship between these abstractions and the development of hydraulic head depressions was conducted considering the hydrogeological complexes (aquifer units), and the water bodies involved (defined by the GDWR-BI). Rainfall and pumping data were compared with the evolution of hydraulic heads measured in the monitoring network for groundwater supply of the GDWR-BI.

### 3.2. Groundwater sampling and profiling of EC with depth

Different tasks were performed in wells of the monitoring network of the GDWR-BI and in the Sa Gleda-Camp des Pou cave (Figs. 1B, 2B) to obtain data for the study of the spatial and temporal position of the freshwater-seawater interface. These tasks were the following: i) in June–July 2022, in 26 wells of the GDWR-BI network, a field survey was undertaken for the measurement of groundwater piezometric levels, determination of physicochemical parameters and analyses of chemistry and multi-isotopes from groundwater samples in the laboratory; ii) in August 2022, another survey was conducted in two separate zones within the Sa Gleda-Camp des Pou cave at 3 different depths (above the halocline, at the halocline, and at the bottom of the cave) in 6 points taking a total of 18 water samples (Fig. 2B, depth profiles 1G, 2G, 3G, 5G, 6G, and 7G) to determine, in the laboratory, the same parameters as in the well samples of the GDWR-BI monitoring network (Table SI–3 of the SI document shows the position with respect to the halocline of each of the water samples); iii) in addition, in July–September 2022, depth profiles of temperature (T, °C) and electrical conductivity (EC, mS/cm) of the groundwater were also recorded in piezometers of the GDWR-BI hydraulic head monitoring network (Fig. 1B); and iv) furthermore, from the historical record of wells sampled from the GDWR-BI monitoring network, past water quality data of these were collected. The SI document contains the information on the sampling protocols followed in the monitoring network and in the Sa Gleda-Camp des Pou cave.

For the study and interpretation of hydrochemical and isotopic results obtained in the 26 wells sampled from the monitoring network, data were grouped according to transects subparallel to the main NW-SE fracturing direction (Fig. 1B), perpendicular to the coastline. Table SI–4 of the SI document lists some of the main characteristics of the measurements and sampling wells. In this table, wells that exploit waters from the Liassic or Upper Triassic dolostones are those located in the Serres de Llevant range area (in fact, most of the wells located in this area exploit waters from these rocks), while wells that exploit waters from the Miocene-Mesozoic contact (calcarenites-dolostones) or from the Upper Miocene (calcarenites) correspond to those located in the Marina de Llevant (Fig. 1B).

As for the six points at each of which three water samples were taken at three depths in the Cave of Sa Gleda-Camp des Pou, these were distributed in the northeastern and southwestern sectors along supposed fractures (Fig. 2B). All the samples from the cave were taken directly by cave diving.

EC and T variation with depth were recorded to characterize the time evolution of the freshwater-saltwater interface, as well as its position and thickness. This task was conducted in 2002, 2012 and 2022 in 8 wells of the hydraulic head monitoring network distributed throughout the study region (wells are marked in purple in Fig. 1B). The measurement interval varied from 10 cm to 30 cm at depths where changes in T and EC were observed, and from 30 cm to 50 cm at depths with constant values (in some cases with intervals of up to 1 m).

Concentrations of major and minor ions and elements were analyzed in the 26 groundwater samples taken from the GDWR-BI monitoring network and the 18 samples taken from the Sa Gleda-Camp des Pou cave. Table 1 shows the analyses conducted and the analytical techniques and instrumental equipment used. The isotopic composition of the water molecule ($\delta^{18}O$ and $\delta^{2}H$) was also analyzed (Table 1), and the values of the isotopic ratio $^{87}Sr/^{86}Sr$ and the value of $\delta^{11}B$ were obtained. In the latter case, the sample purification was conducted at the LIRA laboratory of the University of Barcelona. More details on the purification process and analysis can be found in the SI document.

Groundwater samples were analyzed at the laboratories of the GDWR-BI and at the laboratories of the Scientific and Technological Centers of the University of Barcelona (CCiTUB). More information on characteristics of techniques and protocols used are given in the SI document.

## 4. Results and discussion

### 4.1. Intergranular porosity, fracture framework system, and karst conduits

The main lithologies of the hydrogeological complexes (described in Section 2) are characterized by high intergranular and fracture-fissure porosities. Fornós and Gràcia (2021) provided evidence of the high fracturing of the dolostones of the Mesozoic basement in the Sa Gleda-Camp des Pou cave (photograph B of Fig. 3), as well as of the high porosity of the conglomerates and microconglomerates of the Upper Miocene (photographs C and D of Fig. 3), and of the different moldic porosities of limestones, bioclastic calcarenites of the reef facies materials (Upper Miocene), as for example the bioclastic limestones of Santanyí (photograph E of Fig. 3). Furthermore, the visual analysis of the drill cores from the monitoring wells of the hydraulic head located in the Marina de Llevant has shown a large moldic porosity in the Santanyí limestones (Fig. 3E).

The Serres de Llevant range has been affected by three main tectonic phases (Moragues et al., 2021): pre-alpine distension (Oligocene-Lower Miocene); alpine compression (Middle Miocene), and Miocene distension (Middle-Upper Miocene). The alpine compression is constituted by an imbricated thrusting system majorly verging towards the NW (although also W and SW), whose detachment level is located in the

**Table 1**
Analyses conducted on the groundwater sampled in the control and monitoring network of the GDWR-BI and in the Sa Gleda-Camp des Pou cave. Techniques used are also included.

| Analyzed parameters, ions and isotopes | Physicochemical parameters determined T, DO, EC, ORP and pH |
|---|---|
| Ions and isotopes | Analytical techniques |
| Major anions $Cl^-$ and $SO_4^{2-}$ | High Performance Liquid Chromatography (HPLC), according to EPA 9056 |
| Major anion $HCO_3^-$ | Ion Titration, according to Standard Methods 2320 |
| Major cations $Ca^{2+}$, $Mg^{2+}$, $Na^+$ and $K^+$ | Inductively Coupled Plasma-Optical Emission Spectrometry (ICP-OES), Optima 3100, Perkin Elmer, Waltham, MA, USA according to EPA Method 6010D |
| Minor elements Sr and B | Inductively coupled plasma-mass spectrometry (ICP-MS), Elan 6000, Perkin Elmer, Waltham, MA, USA, according to US EPA Method 200.8 |
| $\delta^{18}O$, $\delta^{2}H$ (water molecule) | Isotopic ratio mass spectrometry (IRMS), Delta Plus XP2, with TCA-EA pyrolyzer and Carlo Erba 1108 elemental analyzer; and for samples with higher salinity, the Picarro L2130 technique with HDS-2412 vaporizer |
| $^{87}Sr/^{86}Sr$ ratio and $\delta^{11}B$ | Plasma mass spectrometry (ICP-MS) once purification of the samples at the Laboratory of Radiogenic and Environmental Isotopes (LIRA) of the University of Barcelona |

Triassic Keuper facies materials (Sàbat et al., 2011; Moragues et al., 2021). The Oligocene and Miocene normal faults show two main directions (NE-SW and NW-SE), thus constituting an orthogonal fracture system that compartmentalizes the study region (Fig. 3F) in horsts and grabens (Moragues et al., 2021).

As the Marina de Llevant rocks are younger than the alpine compression, they are only affected by the Miocene distension. As a result of this geological evolution, the geomorphological present-day features are conditioned by the NW-SE and NE-SW normal faults, which compartimentalize the region and condition the coastline and main dry streams.

The aforementioned main fracturing directions also condition the groundwater flow associated with dry streams (Fig. 3F), which are mostly oriented NE-SW and NW-SE (Céspedes et al., 2001; Giménez et al., 2002). In addition to the orthogonal fracture system, the mapping of underwater karst caves allowed the identification of other less penetrative fracture systems (Figs. 2B and 3F).

In the porous host rock matrix of the Mesozoic dolostones and limestones forming the hydrogeological complexes of the Serres de Llevant range, fracture-fissure porosity (Fig. 3 photograph B) prevails over intergranular porosity. In contrast, in the Marina de Llevant, both intergranular porosity (Fig. 3 photographs C, D and E) and fracture-fissure porosity coexisted as host rock matrix. As a whole, the high intergranular and fracture-fissure porosities constitute a permeable network, which is hydraulically connected with the karst network of conduits and control the groundwater flow by double porosity (in the Serres de Llevant, fractures-fissures and conduits), and by triple porosity (in the Marina de Llevant, intergranular matrix, fractures-fissures and conduits). Moreover, Fig. 3F shows the main orientations of the karst cave alignments distributed along the coastline (rose diagrams in Fig. 3F show that directions are N-S, NE-SW, and NW-SE). In particular, in the coastal cave of Sa Gleda-Camp des Pou, the predominant directions are N-S and NE-SW.

In addition to intergranular and fracture-fissure porosity, the aquifer system also has other underwater caves along the coastline (Fig. 3F) and numerous karst conduits that are often exploited by supply wells. This is the case, for example, with the supply wells distributed along transect P6 in Fig. 1B. In the SI document, Fig. SI–2 shows some photographs of karst conduits and the different parts of the Sa Gleda-Camp des Pou cave. The connectivity between the karst conduits and the matrix of the host rock, formed by the intergranular porosity and the fracture system (which involves the fracture-fissure porosity), is evidenced in the piezometric map of July 2022 (see Fig. 3F and Section 4.2.1).

### 4.2. Hydrodynamics of the system related to global and climate change

#### 4.2.1. Functioning of the double-flow system

The main flow direction in the Serres de Llevant-Marina aquifer system is from NW to SE. The hydraulic head map of the Marina de Llevant, obtained on the basis of the field survey carried out in July 2022 (Fig. 3F), showed that the zones where the dry streams are situated (from Serres de Llevant range to the Marina de Llevant) coincide with the predominant fracturing direction in the Serres de Llevant range (NW-SE). There is a preferential flow of groundwater along these fractures and dry streams. The fractures constitute a zone of weakness in the limestones, which causes the streams to be incised into the rock coinciding with zones of high transmissivity. This high transmissivity is attributed to the existence of karst conduits along the fractures. As a result, there is an exchange of groundwater and solutes between the matrix of the host rock and the karst conduits, which act as drainage lines. This behavior is similar to what was observed by Martin and Screaton (2001) in Florida (USA) and Doctor et al. (2006) in Slovenia. This exchange depends on the relationship between the hydraulic head and the top of the karst conduits, as Martin and Screaton (2001) described. Thus, in the Mediterranean climate of Mallorca Island, during summers and winters, periods of low rainfall and low aquifer recharge (or during periods of prolonged drought), hydraulic head is below the top of the conduit. The exchange takes place from the host rock matrix to the conduits because a hydraulic gradient from the porous host rock matrix to the karst conduits is in place (Martin and Screaton, 2001), including the host rock matrix connected to the karst conduits at the freshwater-seawater interface (Neven and Sorab, 2021). This proves that the double-flow in coastal karst aquifers is an additional factor contributing to the deterioration of groundwater quality as the freshwater-seawater interface advances inland during extended drought periods or when extractions increase, which demonstrates the validity of the first working hypothesis (see in the SI document Figs. SI–4 and SI–5 with two examples of the evolution over time of chloride concentrations as a result of the saltwater intrusion process). Conversely, when the hydraulic head rises above the top of the conduits during periods of heavy rainfall (especially when extreme events occur), karst conduits can transfer water and solutes into the host rock matrix, causing a generalized rise in hydraulic heads in a short time interval (Martin and Screaton, 2001). This increase does not last for a long time as the karst conduits quickly drain the groundwater and the hydraulic heads drop back below the top of the conduit, which reverts these conduits back to drainage lines (Martin and Screaton, 2001).

Fig. 4A shows the isotopic composition of the water molecule ($\delta^{18}O$ and $\delta^{2}H$) of groundwater samples from 26 wells of the GDWR-BI network in the study region and from the Sa Gleda-Camp des Pou cave waters. Fig. 4B is a close-up view of a portion of Fig. 4A corresponding to the GDWR-BI network well waters. This figure also provides evidence for the existence of the piston-type model in the Serres de Llevant-Marina de Llevant aquifer system. Thus, in addition to most of the 26 wells in Fig. 4B aligning along the local meteoric water line ($\delta^{2}H = 7.9\ \delta^{18}O + 12.5$), it would be noted that groundwater of many of the samples from wells located in the Serres de Llevant range are grouped in the same elliptical area of the local meteoric water line in Fig. 4B. In this area of the figure, dispersion in the isotopic values is little, varying from −6.2 to −5.5 ‰ in $\delta^{18}O$ ($\Delta\delta = 0.7$ ‰), and from −35 to −31.1 ‰ in $\delta^{2}H$ ($\Delta\delta = 3.9$ ‰), and therefore showing similar recharge elevations.

This agrees with the fact that the recharge elevations in the Serres de Llevant range have low variability, oscillating from 200 to 400 (although in some places it is up to 500 m). An altitude recharge line of groundwater as a function of the isotopic composition of water sampled in the 26 wells of the GDWR-BI monitoring network was not available. However, map of Fig. 4D, which plots the location and topographic elevation where these wells were drilled, combined with the $\delta^{18}O$ and $\delta^{2}H$ values of these groundwaters allowed us to differentiate two clusters of wells in the Serres de Llevant range. Firstly, the wells closer to the higher elevation zones (such as the wells with code numbers 8, 11, 12, 18, and 25 in Fig. 4D) are those whose groundwaters are characterized by lighter isotopic signatures in the elliptical area of Fig. 4B, similar to what was observed by Carmona et al. (2004) and Sappa et al. (2018). Secondly, there are wells located at lower topographic elevations (and whose groundwaters are not mixed with marine waters), which are aligned along the local meteoric water line in the elliptical area of Fig. 4B showing heavier isotopic compositions; these are the wells with codes 2, 3, 4, 7, and 26 in Fig. 4D. The fact that these are heavier groundwaters indicates that they are fed by lower elevation recharge zones. The uniformity in the recharge altitude of groundwater of each of the two groundwater clusters and the well-defined karst conduits, fractures and fissures of the Serres de Llevant range suggest that the flow follows a piston-type model. In the zones where these waters have been recharged, the conduits collect the precipitated rainfall, and with a similar velocity and little mixing between waters (Balacco et al., 2022), they conduct groundwater towards the Marina de Llevant.

In the case of the Marina de Llevant, among the wells whose waters do not result from mixing with seawater, those of codes 3, 5, 6, and 23 (Fig. 4B,D) stand out because they are wells whose waters are heavier than those in the Serres de Llevant range. The great variability in the isotopic composition of these waters indicates that they proceed from recharge zones located at different altitudes in the Serres de Llevant and the Marina de Llevant, similar to what was observed by Bryan et al. (2020) in coastal aquifers in western Australia. These would be waters that in some cases have been recharged in the Serres de Llevant range but mixed with waters recharged in the Marina de Llevant at altitudes ranging between approximately 50 and 20 m (Fig. 4D). This also occurs in samples showing mixing in different proportions with seawater, as the mixing lines start from waters recharged at different elevations distributed along the local meteoric water line, according to Clark (2015). This pattern demonstrates that in the Marina de Llevant the flow model results from a combination of a piston-type flow through the karst conduits in the Serres de Llevant range and an exponential mixing-type flow (Fig. 4B), since the karst conduits in the Marina de Llevant receive groundwater from the host-rock matrix through the intergranular porosity connected with the fracture-fissuring network (Fig. 3B,C,D,E), resulting in a double-flow model.

Moreover, since these porosities are high, due to the nature of the host rock, the pore throat size does not necessarily have to be homogeneous. Thus, in the case of intergranular porosity, it consists of two types of pores: i) well interconnected pores through which solutes transported by groundwater freely move with predominantly advective flow, and ii) smaller and not so well interconnected pores (fine porous matrix), through which groundwater flows much more slowly, and even extremely slow, for example, through micropores partially or totally filled with clays. Solutes reach these pores with a dominantly diffusive flow concentration-gradient driven and described by the Fick's First law.

The existence of the double-flow model is also evidenced in Fig. 4C, where the variability of the $\delta^{18}O$ and $\delta^{2}H$ values of waters of the Sa Gleda-Camp des Pou cave is presented. Thus, in the southwestern sector of the cave (Fig. 2B), where waters are less saline than those of the northeastern sector, these are grouped in the area corresponding to the groundwater of the Marina de Llevant in Fig. 4C,D. In contrast, waters of the northeastern sector are more saline and heavier. Furthermore, in this sector, it is observed that waters with the same salinity (i.e., with the same mixing percentage with seawater) have been recharged at different altitudes (because they have different positions on the local meteoric water line), which agrees with the double-flow model.

#### *4.2.2. Hydraulic head evolution and effects of global and climate change on the groundwater availability*

The annual rainfall evolution in the AEMET weather stations (WS) of the study region (Fig. 5A: WS-A1, WS-A2, and WS-A3) shows how, during wet years, the decrease in rainfall was more significant than in non-wet years, ranging between 150 and 250 mm in the wet years, and between 20 and 100 mm in the non-wet years. Regarding the significance of this decline, the analysis of rainfall data for the period 1950–1975 in the three WS within the study region revealed that the average rainfall during wet years constituted 73 % of the total rainfall. In contrast, this proportion had declined to 56 % for the period 1950–1975 and further decreased to 49 % for the period 1976–2021. Additional details on this calculation are provided in the SI document. These declines in annual rainfall are a consequence of climate change, considering that they are the result of an analysis based on a time data series from three weather stations across the study region (see Fig. SI–1 in the SI document the statistical differences in annual rainfall between the three weather stations used) covering continuous observations between 70 and 90 years up to the present, and corroborate what was already observed by Homar et al. (2010) on the scale of the whole island and are consistent with a significant decline in the recharge of the hydrogeological complexes.

Fig. 5A also shows differences in the decrease in annual rainfall between the AEMET weather stations located in the Serres de Llevant range in Manacor (Sant Crespí Vell, WS-A1) and to a lesser extent in Felanitx (Far de Porto Colom, WS-A2), compared to the station located in the Marina de Llevant in Santanyí (S'Alqueria Blanca, WS-A3). Thus, during the wet years, more rainfall was observed in the Serres de Llevant range than in the Marina de Llevant (Fig. 5A, WS-A1 and WS-A3, respectively). In contrast, in the non-wet years, no significant differences were appreciated between the Serres range and the Marina de Llevant (see Table SI–2 in the SI document). In Fig. 5A, weather stations WS-A1 and WS-A3 also show how the annual rainfall in the area of Manacor village (WS-A1), north of the study region, is higher than the rainfall recorded in Santanyí, located south of the study region, and therefore, the recharge in the latter area was lower.

To analyze the time evolution of the groundwater abstractions in Marina de Llevant (mostly intended for drinking water supply, and especially for the tourism sector, which is very significant in the Marina de Llevant), the territory was structured and divided into six water bodies managed by the GDWR-BI (Fig. 5B), and according to the territorial and hydrogeological criteria indicated in Section 3.1. Fig. 5C1 presents the evolution of these abstractions for the study region (Serres de Llevant range and Marina de Llevant). Although it should be considered that in 2020 and 2021, tourism activity in the coastal areas was lower due to the COVID pandemic, the figure shows that

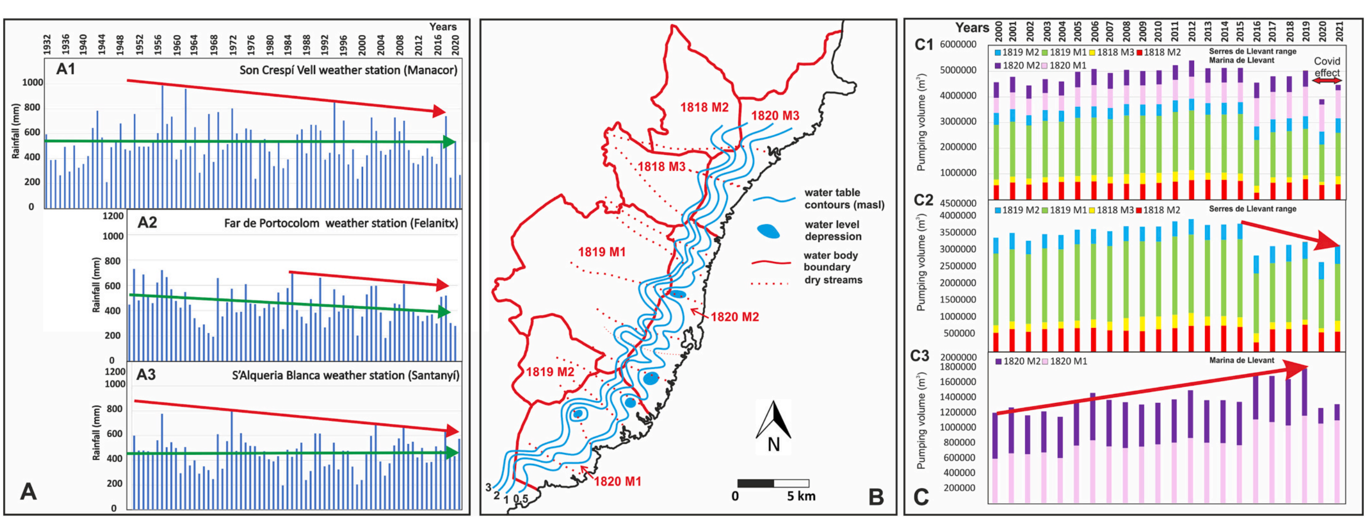


**Fig. 5.** (A) Evolution of annual rainfall in the AEMET weather stations in the study region: (WS-A1) Son Crespí Vell (Manacor), (WS-A2) Far de Porto Colom (Felanitx), (WS-A3) S'Alquería Blanca (Santanyí). (B) Hydraulic head map of the study region (July 2022) and the geographical limits of the water bodies managed by the GDWR-BI. (C) Time distribution of groundwater abstractions in all water bodies of the study region (C1), in the water bodies of the Serres de Llevant range (C2) and in the water bodies of the Marina de Llevant (C3).

abstractions were progressively increasing from 2000 to 2015, increasing afterwards until the pandemic (Fig. 5C1). However, the increase was especially significant in water bodies 1820 M1 and 1820 M2 (Fig. 5C3), in the south of the Marina de Llevant (from 2000 to 2019), where significant hydraulic head depressions formed (similar to depressions in 2022, Fig. 5B). Related to this, the hydraulic head map of Fig. 3F shows how these major depressions are located in areas where karstic conduits occur (following the trace of supposed faults-dry streams), similar to what was observed by the models of Kresic and Panday (2021). From 2020 to 2021, the pumping extraction drastically decreased due to the COVID pandemic effect (Fig. 5C1).

A similar analysis of abstractions was performed in the case of the Serres de Llevant range (water bodies 1819 M1 and 1819 M2, 1818 M2 and 1818 M3). Fig. 5C3 shows that abstractions increased from 2000 to 2015 and subsequently decreased. The time evolution of the hydraulic heads in the wells of the GDWR-BI level control network is characterized by the effect of climate change (manifested, for example, through decreased recharge) and global change (manifested, for example, through increased abstractions) on the values of the hydraulic heads. Thus, the hydraulic head control wells located in the Serres de Llevant range, which are closer to the water recharge zone, showed greater level oscillations than those located in the Marina de Llevant.

During wet years in the Serres de Llevant range, the recorded level oscillations varied between 0.9 and 1.5 m, while in dry years, they oscillated between 1.5 and 2.5 m. A progressive increase in these oscillations up to 2017 is visible, which is associated with the progressive increase in the abstractions in the Serres de Llevant range (Fig. 5C2).

In contrast, in the Marina de Llevant, the piezometric level oscillations in the upper and lower hydrogeological complexes (see in Section 2, the Marina de Llevant study region) were smaller given the proximity to the natural discharge zone, corresponding to the coastline (Srzić et al., 2020). The upper hydrogeological complex has maintained fairly constant level oscillations since 2010 (ranging between 0.25 and 0.3 m, Fig. 6A2), coinciding with a sustained hydraulic head recovery as a result of the decrease in abstractions as a consequence of the quality decline of groundwater resources in the area monitored by section S22-A of monitoring well S22 (this monitoring section corresponds to the upper hydrogeological complex, see figure caption of Fig. 6A). In contrast, in the lower hydrogeological complex, oscillations increased, especially in dry years (varying between 0.3 and 0.4 m) and coincided with a progressive decrease in maximum and minimum hydraulic heads (see in Fig. 6A1, the hydraulic head oscillation in the corresponding section of the monitoring well, S22—B). This progressive decrease in levels is associated with the increase in abstractions recorded in the Marina de Llevant, especially in the 1820 M1 and 1820 M2 water bodies (Fig. 5B). The first water body is where the control well S22 is located and, together with the second water body, is where significant pumping depressions have been detected (Figs. 3F and 5B).

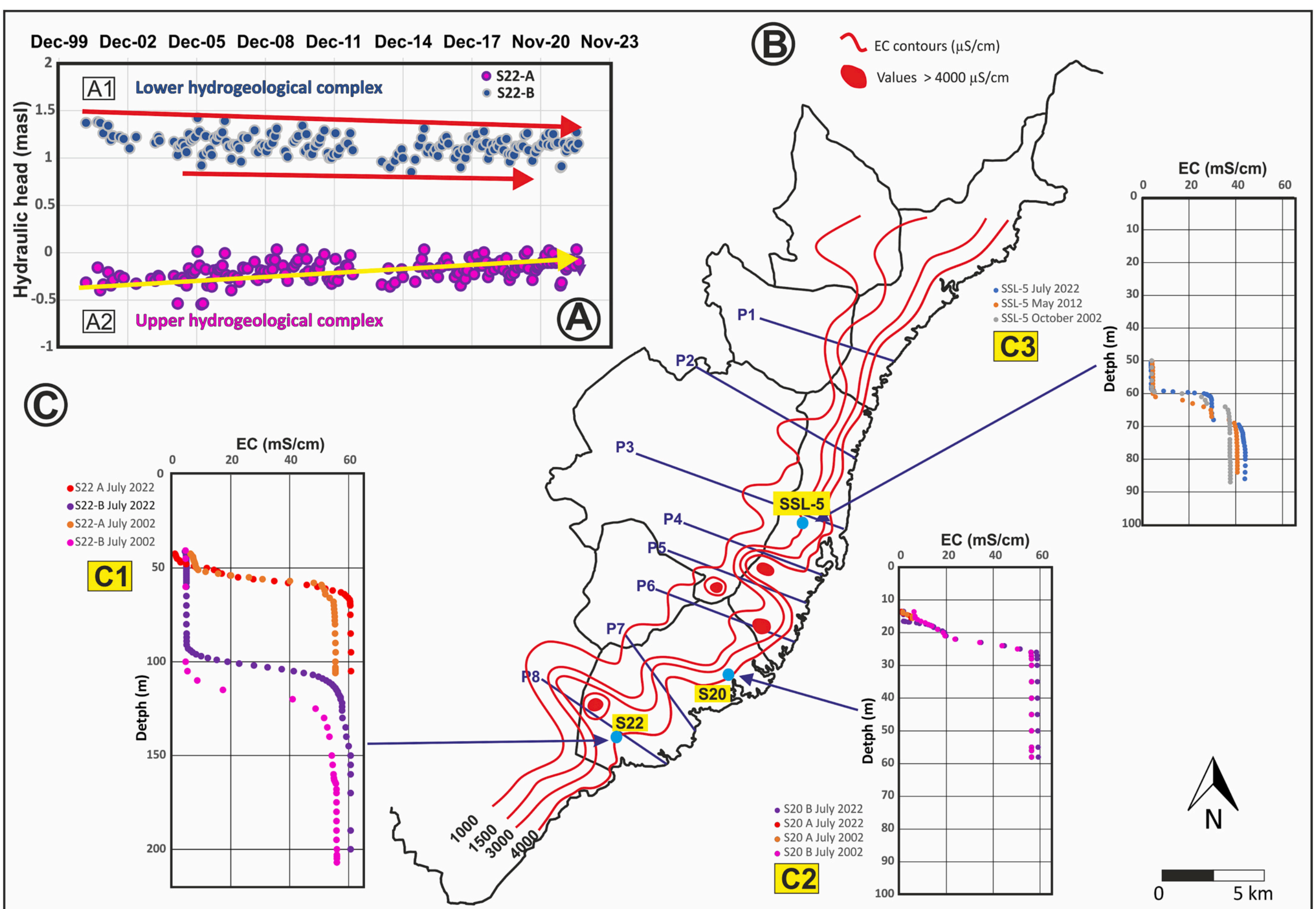


Fig. 6. (A) Time evolution of piezometric levels in monitoring well S22, located in the Marina de Llevant (Santanyí area). This monitoring well controls, in addition to the piezometric levels, the electrical conductivity with depth of the unconfined upper aquifer (upper section S22-A of this well) and the lower aquifer (deep section S22—B of the well). The lower aquifer is confined in the Santanyí area by a 15 m level of clays (see Section 2). (B) Map of electrical conductivitiy of the Marina de Llevant (July 2022). (C) Time evolution of electrical conductivity log profiles in three selected monitoring wells: C1 (S22), C2 (S20) and C3 (SS-L5).

### 4.3. Seawater intrusion in the Serres de Llevant-Marina aquifer system

#### 4.3.1. Position of the freshwater-seawater interface and evolution over time

The map of the electrical conductivity in July 2022 in the Marina de Llevant (Fig. 6B) reveals the spatial distribution of the penetration of the freshwater-seawater interface. This map highlights an uneven penetration of the interface and the relationship of this penetration with the degree of abstraction of the hydrogeological complexes. Thus, the greatest interface penetration (Fig. 6B) occurred in water body 1820 M1 (Fig. 5B) where the following elements converged to explain this major penetration of the interface: i) a progressive increase in groundwater abstractions was recorded to date (Fig. 5B3), ii) rainfall has been declining (Fig. 5A3), iii) significant hydraulic head depressions occurred (Fig. 5B), and iv) salt-water domes have formed (Fig. 6B), similar to what was observed by Panthi et al. (2022).

Furthermore, EC log profiles with depth corresponding to the monitoring well S22 (Fig. 6C1), located in the water body 1820 M1 (Fig. 5B), shows how the mixing zone between freshwater and seawater in the upper hydrogeological complex (monitoring well section S22-A) was situated between 43 and 66 m depth (23 m thick) in July 2022. The position of the interface is similar as in 2002 (Fig. 6C1), which agrees with the mentioned progressive level recovery (Fig. 6A2) that occurred in this monitoring well because of the suspension of abstractions in the area (see Section 4.2.2). In contrast, the EC log profile in the deep hydrogeological complex (Fig. 6C1) monitoring well section S22—B shows that the mixing zone is located between 94 and 122 m depth (28 m thick), therefore at a shallower depth than in 2002, in accordance with the increased abstraction of the deep hydrogeological complex in this area (see Section 4.2.2) and with the progressive decline in levels of this hydrogeological complex (Fig. 6A1). All this leads to the freshwater-seawater interface penetrating more than 8 km from the coast.

Water body 1820 M2 (Fig. 5B) is another sector where a clear penetration of the freshwater-seawater interface was detected (Fig. 6B), preferentially through a strip in which there was strong abstraction and where a significant and generalized hydraulic head depression accompanied by salt-water domes was detected (Figs. 3F and 6B, respectively). The EC log profiles with depth in the SSL-5 monitoring well located in this zone (Fig. 6C3) also revealed the occurrence of two depth intervals of different thickness corresponding to two water mixing zones: one corresponding to the upper hydrogeological complex (located between 59 and 61 m) and the other to the deep hydrogeological complex (located between 67 and 71 m depth). In both cases, the thickness of the mixing zone was lower than in the case of the EC log profile of monitoring well S22. This would indicate that the SSL-5 monitoring well intercepts two karst conduits, hence two depth intervals with high transmissivity. The medium is very heterogeneous in the surroundings of this monitoring well, with recorded transmissivities of up to 2500 $m^2$/day. These high transmissivities favor a significant interface penetration and mixing zones of smaller thickness (Custodio, 2013) than in S22, where the EC log profile of monitoring well S22 (Fig. 6C1) displayed thicker mixing zones (23 and 28 m thick in the upper and deep hydrogeological complex, respectively) and lower transmissivity, according to the fact that this monitoring well was excavated in a host rock in which the matrix porosity was of intergranular and fracture-fissure types.

In Fig. 6C3, the EC log profile of monitoring well SSL-5 also shows that, unlike what was observed in section S22-A (upper hydrogeological complex) of monitoring well S22, the freshwater-seawater interface in the upper hydrogeological complex is at a shallower depth than in 2002 and 2012, indicating greater penetration of seawater intrusion. On the contrary, in the deep hydrogeological complex, in 2002, the interface was at a shallower depth (64 m) than in 2022 (78 m), indicating that, in this latter case (Fig. 6C3), the intrusion had moved to the coast. This is in accordance with a decrease in the abstraction of the unconfined dolostones and limestones hydrogeological complex of the Serres de Llevant range. This highlights the good hydraulic connectivity between the hydrogeological complex of the Mesozoic basement (Serres de Llevant range) and bioclastic calcarenites of the Miocene (Marina de Llevant, see Section 2).

In the past when the seawater intrusion began to advance inland in this sector of the Marina de Llevant, a concentration gradient of solutes (including chloride) occurred. This gradient was established between the saltwater in the well-interconnected pores of the zone, which were already invaded by seawater, and the still unaffected water in the pores whose pore throat size was smaller and less well-interconnected (see Section 4.2.1). Similarly, another analogous concentration gradient was established at the contact between the saline intrusion advancing front and the host rock still unaffected by the intrusion. These gradients resulted in the solutes, including chloride, penetrating into the host rock matrix by molecular diffusion and being stored within the finer porous matrix.

During prolonged drought periods, such as those already occurring because of climate change (see Section 4.2.2), the deficit in aquifer recharge increases the progression of the seawater intrusion process. This is an adverse environmental impact resulting from the coupling of climate change and global change (high abstractions due to the need to provide water of suitable quality to meet the needs of the tourism and agricultural sectors) that is aggravated by the double porosity characteristic of the double-flow model along the conduits and through the porous host-rock when saltwater advances inland (see the first hypothesis).

Furthermore, in addition to the mentioned prolonged droughts, the climate change scenario for the Mediterranean region foresees the occurrence of extreme rainfall events (Teotónio et al., 2020) (in fact, they are already occurring on a regular basis). In such events, there is an increase in recharge and a subsequent regression of seawater intrusion. In this case, the flow of fresh groundwater to the sea results in a chloride flushing of the well-intercommunicated pores of the double porosity. However, this is not the case for the finer pores, where a substantial amount of chloride and other solutes remains trapped within. These solutes slowly mobilize through molecular back-diffusion contaminating the well-connected pores. This refers to the rebound effect, which occurs when back-diffusion is overlooked when designing the aquifer remediation. This is what observed Puigserver et al. (2013, 2016, 2022) in aquifers in granular media with different hydraulic conductivities, and Syafiuddin et al. (2020) and Guo et al. (2021) in karst aquifers. As a result of the rebound effect, abstraction wells continue to extract groundwater with concentrations exceeding the allowable limits for the intended purposes. Fig. SI–4 in the SI document illustrates the back-diffusion process in the upper hydrogeological complex in the Marina de Llevant. In this case, a sustained decrease in chloride concentrations was observed in a well from the GDWR-BI monitoring network. This decline coincided with a reduction in groundwater abstractions from the hydrogeological complex. Although these abstractions were not completely eliminated, they were significant enough for hydraulic heads to begin to recover (see Fig. 6A2). From Jun-20, there was a progressive increase in chloride suggesting that the cause was the back-diffusion process (rebound effect) as seawater intrusion retreated, thus confirming the second working hypothesis. Again, these adverse effects result from the interaction of climate change and global change in Mediterranean karst areas.

#### 4.3.2. Hydrochemical facies and processes associated with seawater intrusion

Hydrochemical facies of groundwater in the Serres de Llevant-Marina aquifer system varied from calcium bicarbonate or calcium bicarbonate-chloride (Fig. 7A, facies set 1) to calcium-magnesium bicarbonate or calcium-magnesium bicarbonate-chloride (Fig. 7A, facies set 2) in the case of the Serres de Llevant range. Regarding the Marina de Llevant, facies varied from calcium-magnesium bicarbonate-chloride to sodium chloride (Fig. 7A, facies set 3), the latter being those with a higher percentage of water from seawater intrusion (or salt-water

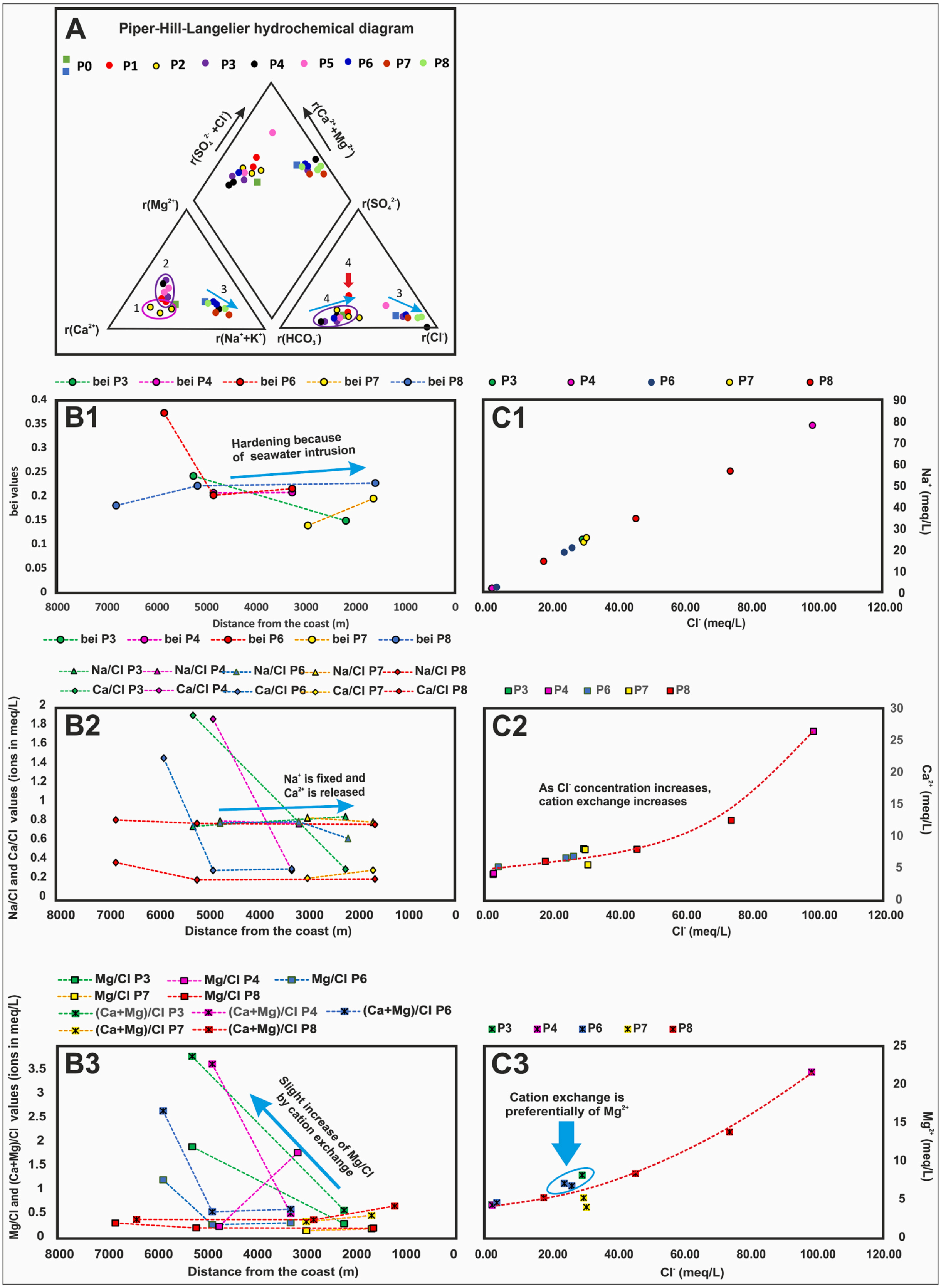


**Fig. 7.** (A) Piper plot of groundwater sampled along transects perpendicular to the coastline in the flow direction (Fig. 1B). (B) Evolution of ionic ratios: base exchange index (bei), calculated as (rCl-r(Na + K))/rCl; rNa/rCl; rCa/rCl; rMg/rCl, and (r(Ca + Mg)/rCl) as a function of distance from the coastline. (C) Evolution of $Na^{+}$, $Ca^{2+}$ and $Mg^{2+}$ concentrations with respect to $Cl^{-}$ concentration.

domes) and subjected to successive evaporation-re-evaporation cycles of irrigation returns.

The calcium bicarbonate to calcium-magnesium bicarbonate nature (facies sets 1 and 2 in Fig. 7A) is evidence of interaction with Jurassic limestones and dolostones, respectively. The fact that groundwater without seawater intrusion has a certain chloride character is related to the recharge zone of the aquifer system being very close to the coast with a contribution from marine aerosols.

Fig. 7A also shows that the hydrochemical transects P6, P7, and P8, from Serres de Llevant range to Marina de Llevant (Fig. 1B), had a higher proportion of samples with a larger percentage of mixing with seawater. These transects are located to the south of the study region, and the following elements converge in them: i) greater number of hydraulic head depressions (Fig. 3F), ii) higher abstraction, and iii) higher salinity (Fig. 6B). The Schoeller-Berkaloff plots (Fig. SI–3A) show how, in the water body 1818 M2 (Fig. 5B) of the Serres de Llevant range, a control well had a higher sulfate content (sulfate hydrochemical facies set 4, Fig. 7A), which suggests that groundwater interacted with Triassic materials of the Keuper facies. Fig. SI–3B shows how seawater intrusion affects wells located in the Serres de Llevant range, coinciding with the formation of salt-water domes caused by the concentration and overlapping of pumping cones (Fig. 6B).

Piper and Schoeller-Berkaloff diagrams indicate the occurrence of cation exchange between $Na^+$ in the sodic clays of the wedge for $Ca^{2+}$ and $Mg^{2+}$ in the clays of the aquifer in sectors affected by seawater intrusion as the wedge advances inland and invades the aquifer (Sun et al., 2023), since $Na^+$ is not in equilibrium during the process of seawater intrusion advance.

In the case of the Sa Gleda-Camp des Pou cave, the predominant hydrochemical facies was sodium chloride, with no cation exchange processes observed. Thus, Fig. SI–3D shows how $Na^+$ and $Cl^-$ are in equilibrium, as it is a cave with less interaction with clayey materials. In addition, as the water mineralization degree increases as a result of a higher proportion of mixing with seawater, the bicarbonate concentration decreases (Fig. SI–3D).

Fig. 7B1,B2,B3 shows the evolution of the ion ratios along the hydrochemical transects from the Serres de Llevant range to Marina de Llevant following a flow line at increasingly closer distances to the coastline (Fig. 1B). As for the base exchange index, it is calculated as follows: bei = (rCl-r(Na + K))/rCl (r being the ion concentration in meq/L, Custodio and Llamas, 1983). This parameter tends to increase from inland to the sea in most of the transects (Fig. 7B1). This agrees with a gradual water hardening towards the coastline as a result of the increased percentage of mixing with seawater, in a similar way as observed by Han et al. (2015). More information on base exchange is given in the SI document.

Fig. 7B2 shows that the rNa/rCl ratio did not show significant changes between the transects in sectors where freshwater dominated and where seawater intrusion was detected (transects P3 and P4). In contrast, a significant decline in the rCa/rCl ratio was detected in the same transects. The figure reveals that changes also occurred as the percentage of freshwater mixing with seawater increased. In the same figure, it is observed how, towards the coast, the rNa/rCl ratio showed a tendency to decrease, while the rCa/rCl ratio tended to increase as a consequence of the cation exchange (described in Eq. 1 in the SI document). This process was also observed in Fig. 7C2, C3. Thus, whereas a practically linear relationship existed between $Na^+$ and $Cl^-$ (Fig. 7C1), the $Ca^{2+}$ and $Cl^-$ relationship was asymptotic, especially with higher water $Cl^-$ concentrations (Fig. 7C2 in P4 and P8). This indicates that the higher the $Cl^-$ concentration, the more the $Ca^{2+}$ concentration increases above expected values due to cation exchange of $Na^+$ for $Ca^{2+}$ according to Eq. 1 (SI document).

The cation exchange process was also evidenced from the evolution of the ionic ratios rMg/rCl and r(Ca + Mg)/rCl as a function of distance from the coastline (Fig. 7B3), which is similar to that described for the rCa/rCl ratio (Fig. 7C2). The plot of $Mg^{2+}$ concentrations with respect to $Cl^-$ (Fig. 7C3) reveals the occurrence of cation exchange of $Ca^{2+}$ and/or $Na^+$ with $Mg^{2+}$ (according to Eqs. 2 and 3 in the SI document). plot of Fig. 7C3 displays that $Mg^{2+}$ concentrations of samples from transects P3 and P6, which showed seawater intrusion (Fig. 7C3), are situated above the asymptotic trend in the evolution of $Mg^{2+}$ concentrations with respect to $Cl^-$. This coincides with a lower $Ca^{2+}$ and $Na^+$ concentration, which suggests the existence of cation exchange according to Custodio and Llamas (1983) and Appelo and Postma (2004).

#### *4.3.3. Evaporation processes of irrigation waters and mixing lines with seawater*

Groundwater samples collected from wells exploiting the upper hydrogeological complex in the water bodies 1820 M1 and 1820 M2 of the Marina de Llevant (Fig. 5B) are represented in Fig. 4B. Although most of waters of that figure are aligned along a local meteoric water line, some of them, which because of their chloride chemical composition show signs of salinization, are well aligned along two parallel evaporation lines. The analytical expressions for these evaporation lines are $\delta^2H = 2.14\ \delta^{18}O$ -18.72 (line L1) and $\delta^2H = 2.14\ \delta^{18}O$ -17.25 (line L2). Intercepting both lines with the local meteoric water line gives the isotopic composition of the original groundwater before evaporation. The isotopic compositions of the original groundwater would correspond to those of the recharge at slightly different elevations. Groundwater along lines L1 and L2 (evaporation lines Fig. 4B) correspond to water for agricultural use and, to a less extent, for water supply. This is evidence of an increase in water salinity occurring in water bodies 1820 M1 and 1820 M2 (Fig. 5B) as a result of the re-infiltration of evaporated water of increasingly heavier isotopic character after repeated irrigation-reinfiltration cycles (irrigation returns, because of the use of the flooding method as the irrigation system). This highlights that the good connectivity in the upper hydrogeological complex of the Santanyí Miocene limestones favors the rapid recharge of the complex with water from irrigation returns (more saline, re-evaporated and re-infiltrated), which increases the salinization of the hydrogeological complex. Furthermore, this also leads to salinization of agricultural soil, similar to what was observed by Ahmed et al. (2013). The sodium adsorption ratio (SAR) is a standard parameter for the quality of water used for agricultural irrigation that is also used to diagnose the sodicity risk of an agricultural soil. The SAR is calculated as follows: $rNa/[(rCa + rMg)/2]^{(1/2)}$ (with r meaning meq/L). When the SAR of an agricultural soil reaches or exceeds a value of 13.0, it is at risk of sodification (USDA, 2012; Aboelsoud et al., 2022; Surinaidu et al., 2023). When this occurs, the soil may show an increase in the dispersion of particulate organic matter and clay particles. This leads to a decrease in saturated hydraulic conductivity, and therefore in soil aeration. All this results in the degradation of the soil structure. In the Marina de Llevant, the SAR value of 13.0 is exceeded in the transect wells located in water bodies where large volumes of groundwater were abstracted (Fig. 5B) accompanied by strong upwelling of salty or brackish water due to the formation of salt-water domes (Fig. 6B). These are mainly transects P8 and P7 (Fig. 6B), in water body 1820 M1 (Fig. 5B), and transect P6 (Fig. 6B), in water body 1820 M2 (Fig. 5B). The calculated SAR values in wells of these transects were above 13.0, ranging from 17.2 to 31.6 (with a mean value of 20.7). In the remaining sampled wells in the eight transects, SAR values were below 13.0, ranging from 1.6 to 11.0 (with a mean value of 3.1). Accordingly, high SAR values above the value of 13.0 in the Marina de Llevant represent a significant negative environmental impact, as it invalidates the productive possibilities of the agriculture soil. This, put in context, is yet another negative environmental impact caused by global and climate change-induced drought.

As for water samples collected at the six sampling profiles at different depths (three samples at each depth profile) in the Sa Gleda-Camp des Pou cave (Table 2), Fig. 4C shows how these waters align along a mixing line with seawater; the equation of this mixing line is $\delta^2H = 6.13 \cdot \delta^{18}O + 3.6$, in accordance with Han et al. (2015). In addition to the mixing line, Fig. 4C also shows the local meteoric water line. The intersection of both

**Table 2**
Percentage of mixing with seawater of samples from the Sa Gleda-Camp des Pou cave. The sample corresponding to the halocline is marked in red.

| | Sampling depth profile | Samples | Mixing percentage with seawater | Sampling depth (m) |
|---|---|---|---|---|
| Southwestern sector of the cave | Sa Gleda 1G | F1-M1 | 35.43 | -8.3 |
| | | F1-M2 | 38.86 | -9.3m |
| | | F1-M3 | 75.43 | -10.3 |
| | Sa Gleda 2G | F1-M4 | 2.29 | -6.3 |
| | | F1-M5 | 14.29 | -7.3 |
| | | F1-M6 | 48.57 | -8.3 |
| | Sa Gleda 3G | F1-M7 | 3.43 | -6.3 |
| | | F1-M8 | 8.57 | -7.3 |
| | | F1-M9 | 48.00 | -8.3 |
| Northeastern sector of the cave | Sa Gleda 5G | F2-M10 | 48.57 | -10 |
| | | F2-M11 | 72.57 | -11.5 |
| | | F2-M12 | 89.71 | -12.5 |
| | Sa Gleda 6G | F2-M13 | 49.71 | -10.5 |
| | | F2-M14 | 72.57 | -11.5m |
| | | F2-M15 | 85.71 | -12.5 |
| | Sa Gleda 7G | F2-M19 | 59.43 | -9 |
| | | F2-M20 | 78.29 | -10.6 |
| | | F2-M21 | 60.57 | -11.5 |

lines gives the original isotopic composition of the cave water ($\delta^{18}O = -5.4 \pm 0.024$ ‰ and $\delta^2H = -31.6 \pm 0.024$ ‰), not yet mixed with marine water (for a seawater that in this part of the coastline has a $\delta^{18}O$ of 1.2 ‰ and $\delta^2H$ of 8.59 ‰) (Dumitru et al., 2017).

Table 2 shows that the southwestern sector of the cave complex had a lower percentage of mixing with seawater than the northeastern sector (Fig. 2B). This is related to fresh groundwater discharges, which are more important in the southwestern sector. Fig. 2B shows the location of the six sampling profiles with depth (three water samples in each profile), distributed in the cave complex and according to the existing fracture network. This figure shows how the Sa Gleda 2 profile (samples F1-M4 to F1-M6) was located next to the intersection between the subparallel contact to the coastline formed by Miocene and Mesozoic rocks and a NW-SE fracture. As previously stated in Section 4.2.1, this fracture direction is one of the main directions of the karst conduits acting as drainage lines, representing the preferential discharge pathways of groundwater, and corresponds to a karst conduit. In the case of Sa Gleda 3 (samples F1-M7 to F1-M9), the lower percentage of mixing with seawater (Table 2) is related to the fact that in addition to being located close to the direction of the previously mentioned karst conduit, it is located downstream of a fracture subparallel to the coastline and is also located in an area with high porosity, as shown in Fig. 2B.

On the contrary, in the northeastern sector (Fig. 2B), following the NW-SE fracturing direction, only one fracture was identified, which intersects mostly with N-S fractures, resulting in a lower groundwater discharge from the aquifer. Moreover, the topography of the cave-karst conduits shows that these conduits are narrower in that sector, which globally corresponds to a lower porosity-permeability of the medium and, therefore, a lower transmissivity.

#### 4.3.4. Variation of $\delta^{11}B$ and of $^{87}Sr/^{86}Sr$ in regard to seawater intrusion

The groundwaters of the Serres de Llevant-Marina de Llevant aquifer system have a variable boron isotopic composition ($\delta^{11}B$) in terms of their relationship with seawater intrusion and irrigation water recycling. Thus, in Fig. 8A3, two groups stand out, a first groundwater group (Group 1) characterized by low EC (waters that do not exhibit seawater intrusion) and have a $\delta^{11}B$ isotopic composition of low variability (between 38 and 40 ± 0.37 ‰). A second group (Group 2) displayed EC varying between 3000 and 6300 μS/cm, values that are influenced by seawater intrusion. In addition, significant variability in the boron isotopic composition occurred (with $\delta^{11}B$ values ranging between 37 and 47 ± 0.37 ‰), which coincided with the waters aligning along line L1 mentioned above (see Section 4.3.3 and Fig. 4B). This is related to the fact that the EC is not only associated with water mixing but also with the recycling degree of re-infiltrated water. In addition, the existence of boron from different sources, including fertilizers, cannot be discarded (Bielski et al., 2020) as discussed below. Group 3 of Fig. 8A3 corresponds to groundwater with high seawater influence, associated with salt-water domes as a result of the occurrence of clustering and overlapping of pumping cones located inland (Figs. 3F and 6B). Although in Fig. 8A2, the same water groups were identified, it should be noted that Group 2 exhibited greater variability in boron concentration than the other groups. This confirms that these are waters that, in addition to being mixed with seawater, experienced repeated recycling cycles and became very heterogeneous, which supports that different boron sources associated with the fertilizers used were involved. In fact, several plantations in the Marina de Llevant need boron for their correct development, among them olive trees.

Plots displaying the $^{87}Sr/^{86}Sr$ isotope ratio variation show (similarly to the $\delta^{11}B$ variation plots) that waters influenced by seawater intrusion and also having undergone recycling have lower Sr concentrations and higher variability in the $^{87}Sr/^{86}Sr$ ratio (Group 2) compared to fresh groundwater (Group 1), Fig. 8B2. Fig. 8B3, which depicts the $\delta^{11}B$ values with respect to the $^{87}Sr/^{86}Sr$ ratio, shows how Group 2 is a mix of waters with significant seawater influence (Group 3) and freshwater (Group 1), which confirms that these are mixing waters that have been re-evaporated and recycled.

In the case of waters of the Sa Gleda-Camp des Pou cave, most of the values of $\delta^{11}B$ (between 39.8 and 41.0 ± 0.2 ‰, Fig. 9A1,A2,A3) were close to that of the seawater value. Waters above the halocline in the northeastern sector were an exception to these results, as they are influenced by freshwater discharges from the aquifer and presented variable boron isotopic compositions (between 40.7 and 42.75 ± 0.2 ‰).

Regarding the $^{87}Sr/^{86}Sr$ ratio in waters from the Sa Gleda-Camp des Pou cave, it was close to that of seawater (0.709, Jørgensen et al., 2008; Mao et al., 2020) in the southwestern sector, and close to that of the aquifer in the northeastern sector (with more variable values in the $^{87}Sr/^{86}Sr$ ratios, ranging from 0.70810 to 0.70905, Fig. 9B1,B2), which is also in agreement with a higher freshwater discharge in the northeastern sector than in the southwestern sector (Fig. 9B1,B2).

## 5. Conclusions

The following two conclusions of this study have significant regional implications:

1. The Serres de Llevant range exhibits a piston-flow model within conduits, resulting in homogeneous isotopic and chemical characteristics of the waters, indicating similar recharge altitudes and showing dominant hydrochemical facies.
2. In the Marina de Llevant, high intergranular and fracture-fissure porosities in the host rock leads to a double and even triple-flow model involving karst conduits and interconnected pores, resulting in greater heterogeneity in water isotopic composition and chemistry.

The remaining conclusions have broader scientific implications regarding the effects of global and climate change on coastal karst aquifers and saltwater intrusion that go beyond the scope of the regional study conducted. The conclusions drawn from these broader implications are as follows:

3. In double-flow karst aquifer systems, karst conduits enable water exchange between the host rock matrix and conduits, influencing the

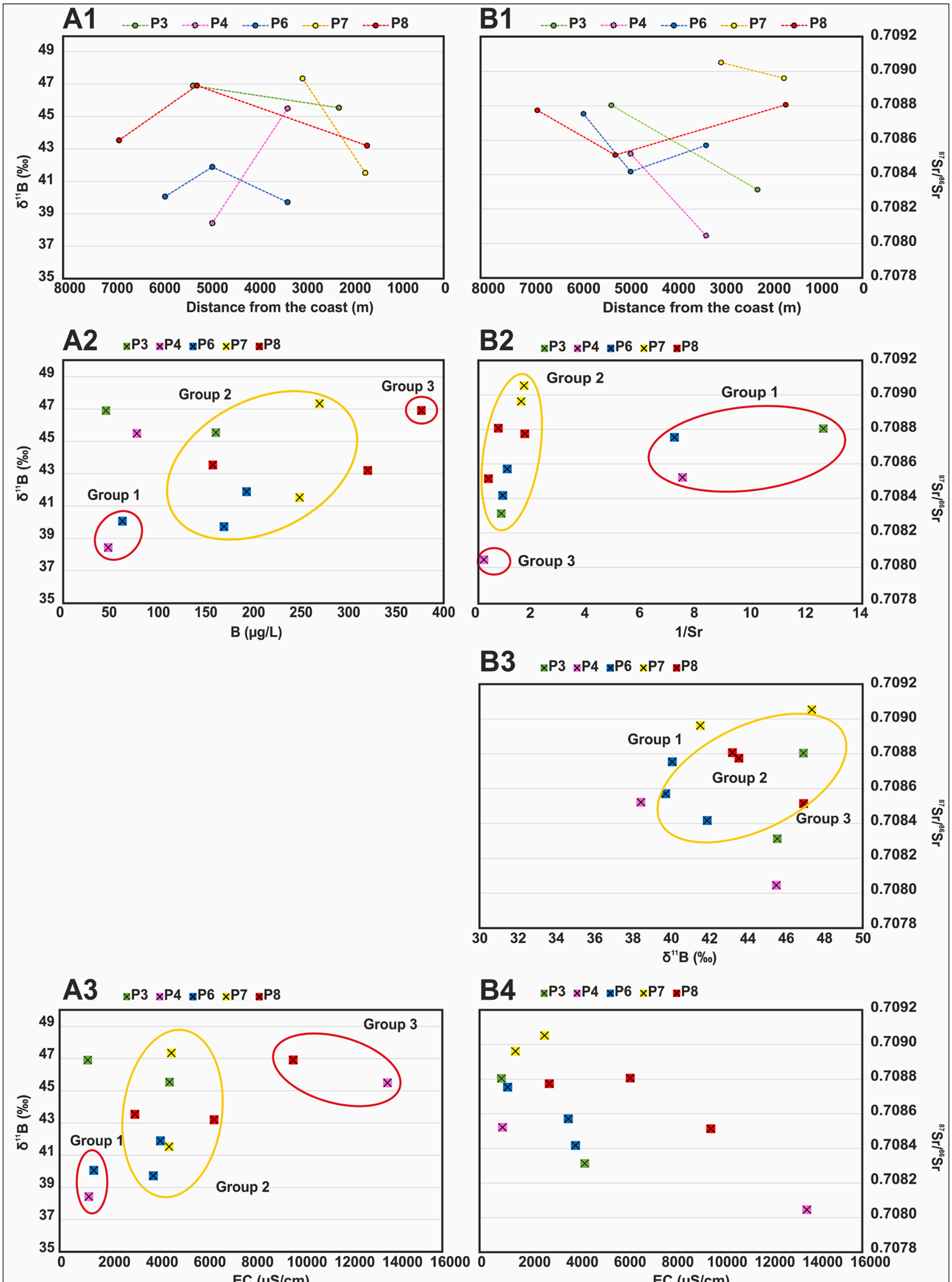


**Fig. 8.** Groundwater sampled at transects P3, P4, P6. P7 and P8. (A) Variation diagrams of boron isotopic composition ($\delta^{11}B$) as a function of the following variables: (A1) Distance to the coastline, (A2) Boron concentration, (A3) Electrical conductivity. (B) Variation diagrams of the $^{87}Sr/^{86}Sr$ isotopic ratio as a function of the following variables: (B1) Distance to the coastline, (B2) Sr concentration, (B3) boron isotopic composition ($\delta^{11}B$), (B4) Electrical conductivity.

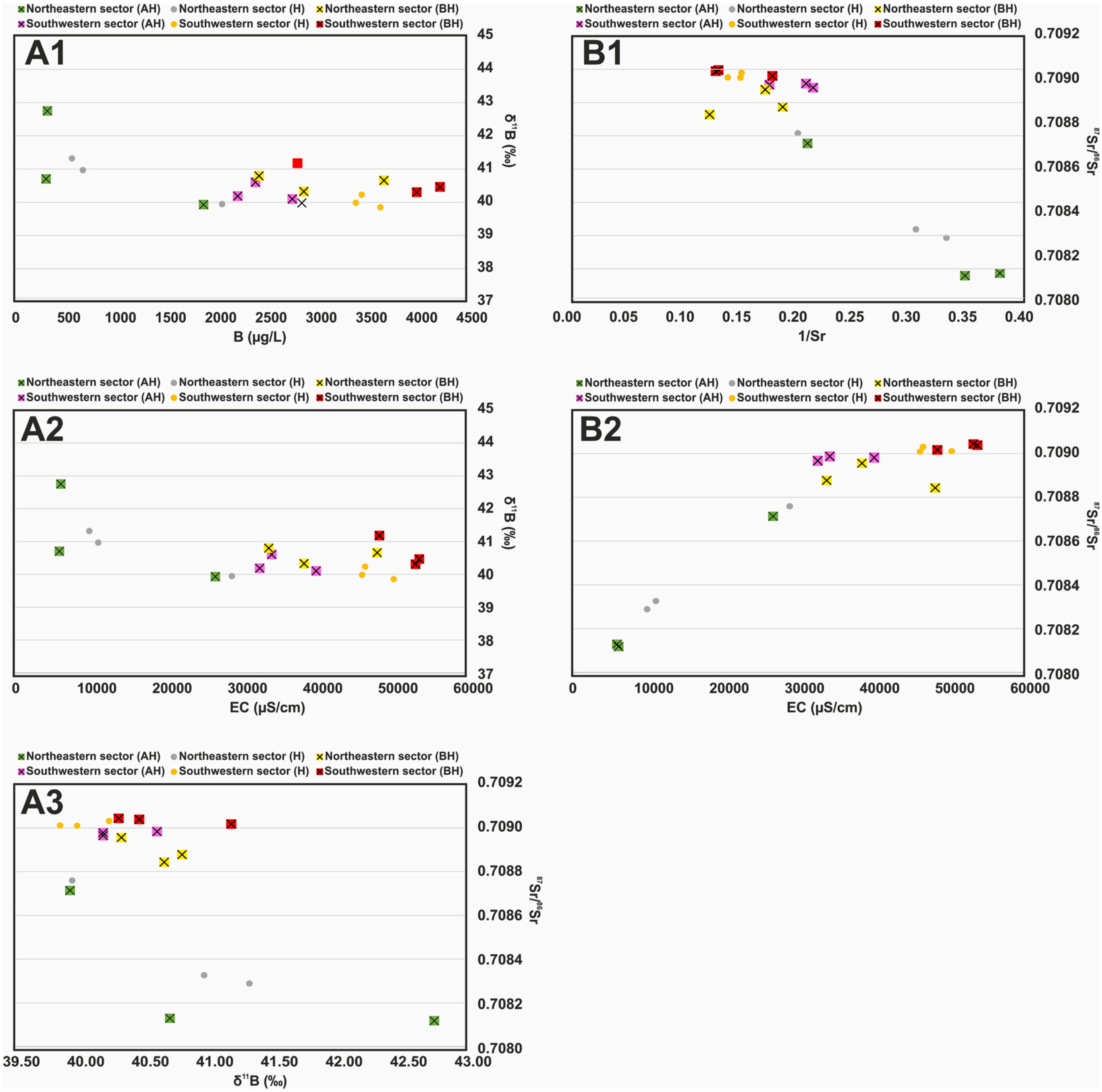


**Fig. 9.** (A) Plots of the variability of boron isotopic composition ($\delta^{11}B$) as a function of the following variables: (A1) Boron concentration, (A2) Electrical conductivity, (A3) Ratio $^{87}Sr/^{86}Sr$. (B) Plots of the variability of the ratio $^{87}Rr/^{86}Sr$ as a function of the following variables: (B1) 1/Sr, (B2) Electrical conductivity.

isotopic and chemical characteristics in the coastal zone and in the entire aquifer system.

4. Changing climatic conditions and increased water abstraction for tourism, driven by global change, are causing seawater intrusion in Mediterranean karst aquifers. This intrusion affects not only coastal areas but also inland regions due to rapid seawater penetration through karst conduits and results in a rapid ascent of the interface, leading to the formation of saltwater domes.
5. The interconnected porosity in the host rock allows solute transport by advection. A portion of this porosity consists of semi-closed or small pores where solutes, including chloride, enter through molecular diffusion and remain stored. This leads to salinity maintenance even after interface regression when pumping ceases. Chloride is then released slowly due to back-diffusion, and the aquifer becomes contaminated again (rebound effect), illustrating the negative impact of climate and global change in a double-flow-dominated Mediterranean karst context.
6. Partial mixing of freshwater with brackish water near the freshwater-seawater interface or saltwater domes can lead to significant issues. If such water is used for agricultural irrigation, it contributes to soil sodification due to the recycling of brackish irrigation runoff. These runoff returns progressively become even more saline, impairing the productivity of agricultural land. This underscores the environmental consequences of the combination of climate and global change in karst coastal regions.

7. Caves in coastal karst aquifers exhibit significant differences in water electrical conductivity and isotopic composition above and below the halocline, highlighting the preferential discharge of continental freshwater associated with karst conduits and the role of fractures in transporting distinct water types.

Finally, it should be noted that the study of coastal karst aquifers is fundamental to understand the impact of global and climate change in climate-sensitive regions such as the Mediterranean. These aquifers are remarkably sensitive to changes caused by global change factors, including increased water abstraction due to tourism, agriculture and industry. They also respond rapidly to the effects of climate change, such as prolonged droughts and heavy rainfall, making them valuable indicators of environmental stress. These aquifers play a key role in the water supply of coastal regions. Their study provides information on how human-induced changes, such as increased water demand and land use modifications, affect groundwater resources. In addition, such studies contribute to understanding how climate change exacerbates these problems, leading to issues such as saltwater intrusion, groundwater contamination, soil sodification and the alteration of water availability. In short, research on coastal karst aquifers in climate-sensitive Mediterranean environments is essential to anticipate and manage the impacts of global and climate change, allowing informed decisions to be made to ensure water resource sustainability and environmental resilience.

## CRediT authorship contribution statement

**Diana Puigserver:** Conceptualization, Investigation, Methodology, Supervision, Writing – original draft, Writing – review & editing. **Jordi Giménez:** Data curation, Resources, Writing – review & editing. **Francesc Gràcia:** Data curation, Investigation, Methodology, Resources. **Àlvaro Granell:** Conceptualization, Data curation, Investigation. **José M. Carmona:** Conceptualization, Formal analysis, Investigation, Methodology, Supervision, Validation, Visualization, Writing – review & editing. **Aina Torrandell:** Data curation. **Joan J. Fornós:** Conceptualization, Formal analysis, Funding acquisition, Investigation, Project administration, Supervision, Visualization.

## Declaration of competing interest

The authors of this research paper (Diana Puigserver, Jordi Giménez, Francesc Gràcia, Àlvaro Granell, José M. Carmona, Aina Torrandell and Joan J. Fornós) declare that they have no known competing financial interests or personal relationships that could have appeared to influence the work reported in this paper.

## Data availability

The authors are unable or have chosen not to specify which data has been used.

## Acknowledgments

The first author wishes to thank Juan Cuerda Barceló for instilling in her the passion to explore the geology of Mallorca. She would also like to thank the members of the Department of Biology (Earth Sciences section) of the University of the Balearic Islands for all their help and for allowing her to participate in their research on the island of Mallorca.

The research team would like to thank Alfredo Barón, geologist and hydrogeologist expert in groundwater resources of the island of Mallorca for his help in the characterization of the hydrogeological complexes of the Serres de Llevant range and the Marina de Llevant.

The research team would like to thank the General Directorate of Water Resources of the Balearic Islands, the Research and Planning Service for facilitating access to recent and historical information, field supervisor Nadal Canyelles for his help in the field work, as well as to the Water Laboratory for their selfless dedication in accommodating increased workload. We would also like to thank the Scientific and Technological Centers of the University of Barcelona (UB) and especially Dr. Leopoldo David Pena of the Laboratory of Radiogenic and Environmental Isotopes of the UB for his help in obtaining the $\delta^{11}B$ and $^{87}Sr/^{86}Sr$ values.

We express our sincere gratitude to the reviewers for their meticulous evaluation and insightful feedback on our scientific manuscript. Their constructive comments significantly contributed to the enhancement of the overall quality of our research.

We also would like to thank the Agencia Estatal de Investigación (AEI), for their support with the research carried out through the project PID2020-112720GB-I00/AEI/10.13039/501100011033.

## Appendix A. Supplementary data

Supplementary data to this article can be found online at https://doi.org/10.1016/j.scitotenv.2023.169246.

## References

Abd-Elhamid, H.F., Javadi, A.A., 2011. Impact of sea level rise and over-pumping on seawater intrusion in coastal aquifers. J. Water Clim. Chang. 2, 19–28.
Aboelsoud, H.M., AbdelRahman, M.A., Kheir, A.M., Eid, M.S., Ammar, K.A., Khalifa, T. H., Scopa, A., 2022. Quantitative estimation of saline-soil amelioration using remote-sensing indices in arid land for better management. Land 11 (7), 1041.
Ahmed, M.A., Abdel Samie, S.G., Badawy, H.A., 2013. Factors controlling mechanisms of groundwater salinization and hydrogeochemical processes in the Quaternary aquifer of the Eastern Nile Delta, Egypt. Environ. Earth Sci. 68 (2), 369–394.
Ambrosetti, Elena, 2020. Demographic challenges in the Mediterranean. MED 300–304.
Antonioli, F., Furlani, S., Montagna, P., Stocchi, P., 2021. The use of submerged speleothems for sea level studies in the Mediterranean Sea: a new perspective using glacial isostatic adjustment (GIA). Geosciences 11 (2), 77.
Appelo, C.A.J., Postma, D., 2004. Geochemistry, Groundwater and Pollution. CRC Press.
Aureli, A., Fidelibusb, D., Priviteraa, A.M.G., Zuppic, G.M., 2006. Salt water intrusion in aquifers of the south oriental coastal zones of Sicily. Environ. Stud. 208.
Aureli, Alice, Ganoulis, Jacques, Margat, Jean, 2008. Groundwater resources in the Mediterranean region: importance, uses and sharing. Water Mediterr. 96–105.
Back, W., Hanshaw, B.B., Pyle, T.E., Plummer, L.N., Weidie, A.E., 1979. Geochemical significance of groundwater discharge and carbonate solution to the formation of Caleta Xel Ha, Quintana Roo, Mexico. Water Resour. Res. 15 (6), 1521–1535.
Bagheri, R., Nosrati, A., Jafari, H., Eggenkamp, H.G.M., Mozafari, M., 2019. Overexploitation hazards and salinization risks in crucial declining aquifers, chemo-isotopic approaches. J. Hazard. Mater. 369, 150–163.
Bailly-Comte, V., Martin, J.B., Jourde, H., Screaton, E.J., Pistre, S., Langston, A., 2010. Water exchange and pressure transfer between conduits and matrix and their influence on hydrodynamics of two karst aquifers with sinking streams. J. Hydrol. 386 (1–4), 55–66.
Bakalowicz, M., 2005. Karst groundwater: a challenge for new resources. Hydrogeol. J. 13 (1), 148–160.
Balacco, G., Alfio, M.R., Parisi, A., Panagopoulos, A., Fidelibus, M.D., 2022. Application of short time series analysis for the hydrodynamic characterization of a coastal karst aquifer: the Salento aquifer (Southern Italy). J. Hydroinf. 24 (2), 420–443.
Barbieri, M., Boschetti, T., Petitta, M., Tallini, M., 2005. Stable isotopes (2H, 18O and 87Sr/86Sr) and hydrochemistry monitoring for groundwater hydrodynamics analysis in a karst aquifer (Gran Sasso, central Italy). Appl. Geochem. 20, 2063–2081 (CrossRef).
Beddows, P.A., Smart, P.L., Whitaker, F.F., Smith, S.L., 2007. Decoupled fresh? Saline groundwater circulation of a coastal carbonate aquifer: spatial patterns of temperature and specific electrical conductivity. J. Hydrol. 346, 18–32 (Return to ref 13 in article).
Behera, A.K., Chakrapani, G.J., Kumar, S., Rai, N., 2019. Identification of seawater intrusion signatures through geochemical evolution of groundwater: a case study based on coastal region of the Mahanadi delta, Bay of Bengal, India. Nat. Hazards 97 (3), 1209–1230.
Bicalho, C.C., Batiot-Guilhe, C., Taupin, J.D., Patris, N., Van Exter, S., Jourde, H., 2019. A conceptual model for groundwater circulation using isotopes and geochemical tracers coupled with hydrodynamics: a case study of the Lez karst system, France. Chem. Geol. 528, 118442.
Bielski, S., Romaneckas, K., Šarauskis, E., 2020. Impact of nitrogen and boron fertilization on winter triticale productivity parameters. Agronomy 10 (2), 279.
Binet, S., Joigneaux, E., Pauwels, H., Albéric, P., Fléhoc, C., Bruand, A., 2017. Water exchange, mixing and transient storage between a saturated karstic conduit and the surrounding aquifer: groundwater flow modeling and inputs from stable water isotopes. J. Hydrol. 544, 278–289.
Biondić, R., Plantak, L., Radovan, A.M., Meaški, H., 2022. Saltwater intrusion of coastal karstic aquifer on the example of the boljkovac water supply pumping Station near Zadar, Croatia. Quaternary 5 (3), 36.

Brenot, A., Négrel, P., Petelet-Giraud, E., Millot, R., Malcuit, E., 2015. Insights from the salinity origins and interconnections of aquifers in a regional scale sedimentary aquifer system (Adour-Garonne district, SW France): contributions of $\delta^{34}S$ and $\delta^{18}O$ from dissolved sulfates and the $^{87}Sr/^{86}Sr$ ratio. Appl. Geochem. 53, 27–41.
Brkić, Ž., Kuhta, M., Hunjak, T., 2018. Groundwater flow mechanism in the well-developed karst aquifer system in the western Croatia: insights from spring discharge and water isotopes. Catena 161, 14–26.
Brown, G.O., 2003. The history of the Darcy-Weisbach equation for pipe flow resistance. In: Environmental and Water Resources History, pp. 34–43.
Bryan, E., Meredith, K.T., Baker, A., Andersen, M.S., Post, V.E., Treble, P.C., 2020. How water isotopes (18O, 2H, 3H) within an island freshwater lens respond to changes in rainfall. Water Res. 170, 115301.
Calligaris, C., Mezga, K., Slejko, F.F., Urbanc, J., Zini, L., 2018. Groundwater characterization by means of conservative (δ 18O and δ 2H) and non-conservative (87Sr/86Sr) isotopic values: the classical karst region aquifer case (Italy–Slovenia). Geosciences 8 (9), 321.
Calvache, M.L., Pulido Bosch, A., 1997. Effects of geology and human activity on the dynamics of salt-water intrusion in three coastal aquifers in southern Spain. Environ. Geol. 30, 215–223. https://doi.org/10.1007/s002540050149.
Capaccioni, B., Didero, M., Paletta, C., Didero, L., 2005. Saline intrusion and refreshening in a multilayer coastal aquifer in the Catania Plain (Sicily, Southern Italy): dynamics of degradation processes according to the hydrochemical characteristics of groundwaters. J. Hydrol. 307 (1–4), 1–16.
Carmona, J.M., Puigserver, D., Font, X., Viladevall, M., Arce, M., Niñerola, J., Ibañez, X., 2004. Hidrogeología y Recursos Hidráulicos, 2. Instituto Geológico y Minero de España - Sociedad Geologica de España, pp. 359–370.
Cary, L., Petelet-Giraud, E., Bertrand, G., Kloppmann, W., Aquilina, L., Martins, V., Pierre, D., 2015. Origins and processes of groundwater salinization in the urban coastal aquifers of Recife (Pernambuco, Brazil): a multi-isotope approach. Sci. Total Environ. 530, 411–429.
Céspedes, A., Giménez, J., Sàbat, F., 2001. Caracterización del campo de esfuerzos neógenos en Mallorca mediante el análisis de poblaciones de fallas.
Chang, Y., Wu, J., Jiang, G., Liu, L., Reimann, T., Sauter, M., 2019. Modelling spring discharge and solute transport in conduits by coupling CFPv2 to an epikarst reservoir for a karst aquifer. J. Hydrol. 569, 587–599.
Chou, M.L., Tseng, H.Y., Wang, C.H., Hseu, Z.Y., 2022. Identification of the water source and groundwater recharge in a paddy field using stable hydrogen and oxygen isotopes. Water Supply 22 (7), 6443–6457.
Cinkus, G., Wunsch, A., Mazzilli, N., Liesch, T., Chen, Z., Ravbar, N., Doummar, J., Fernández-Ortega, J., Barberá, J.A., Andreo, B., Goldscheider, N., Jourde, H., 2023. Comparison of artificial neural networks and reservoir models for simulating karst spring discharge on five test sites in the Alpine and Mediterranean regions. Hydrol. Earth Syst. Sci. 27, 1961–1985. https://doi.org/10.5194/hess-27-1961-2023.
Clark, I., 2015. Groundwater Geochemistry and Isotopes. CRC Press.
Clark, I.D., Fritz, P., 1997. Environmental Isotopes in Hydrogeology. CRC Press, Boca Raton, FL, USA, p. 352.
Costall, A.R., Harris, B.D., Teo, B., Schaa, R., Wagner, F.M., Pigois, J.P., 2020. Groundwater throughflow and seawater intrusion in high quality coastal aquifers. Sci. Rep. 10 (1), 1–33.
Cramer, Wolfgang, et al., 2018. Climate change and interconnected risks to sustainable development in the Mediterranean. Nat. Clim. Chang. 8 (11), 972–980.
Custodio, E., 2012. Coastal aquifer management in Europe. In: Dix huitièmes journées techniques du Comité Français d'Hydrogéologie de l'Association Internationale des Hydrogéologues, 2012.
Custodio, E., 2013. Coastal aquifers. In: Selected Water Problems in Islands and Coastal Areas: With Special Regard to Desalination and Groundwater, 219.
Custodio, E., Llamas, M.R., 1983. Hidrología subterránea, Vol. 1. Omega, Barcelona, pp. 1005–1091.
De Filippis, G., Margiotta, S., Caruso, F., Negri, S.L., 2020. Open questions about the hydrodynamic behaviour of the deep, coastal aquifer of the Salento peninsula (south-eastern Italy): coupling expert knowledge, data, and numerical modelling for testing hydrogeological conceptual models. Sci. Total Environ. 715, 136962.
De Waele, J., Gutiérrez, F., 2022. Karst Hydrogeology, Geomorphology and Caves. John Wiley & Sons.
Doctor, D.H., Alexander, E.C., Petrič, M., Kogovšek, J., Urbanc, J., Lojen, S., Stichler, W., 2006. Quantification of karst aquifer discharge components during storm events through end-member mixing analysis using natural chemistry and stable isotopes as tracers. Hydrogeol. J. 14 (7), 1171–1191.
Dokou, Z., Karatzas, G.P., 2012. Saltwater intrusion estimation in a karstifed coastal system using density-dependent modelling and comparison with the sharp-interface approach. Hydrol. Sci. J. 57, 985–999. https://doi.org/10.1080/02626667.2012.690070.
Döll, Petra, 2002. Impact of climate change and variability on irrigation requirements: a global perspective. Clim. Chang. 54 (3), 269–293.
Dumitru, O.A., Forray, F.L., Fornós, J.J., Ersek, V., Onac, B.P., 2017. Water isotopic variability in Mallorca: a path to understanding past changes in hydroclimate. Hydrol. Process. 31 (1), 104–116.
Duque, Carlos, et al., 2008. Combined time domain electromagnetic soundings and gravimetry to determine marine intrusion in a detrital coastal aquifer (Southern Spain). J. Hydrol. 349 (3–4), 536–547.
Etsias, G., Hamill, G.A., Thomson, C., Kennerley, S., Águila, J.F., Benner, E.M., Flynn, R., 2021. Laboratory and numerical study of saltwater upconing in fractured coastal aquifers. Water 13 (23), 3331.
Feng, Guiping, Jin, S., Zhang, T., 2013. Coastal sea level changes in Europe from GPS, tide gauge, satellite altimetry and GRACE, 1993–2011. Adv. Space Res. 51 (6), 1019–1028.
Ferguson, G., Gleeson, T., 2012. Vulnerability of coastal aquifers to groundwater use and climate change. Nat. Clim. Chang. 2, 342–345. https://doi.org/10.1038/Nclimate1413.
Ford, D., Williams, P.D., 2007. Karst Hydrogeology and Geomorphology. John Wiley & Sons.
Fornós, J.J., Gràcia, F., 2021. Aspectes geològics del sistema espeleològic Gleda–Camp des Pou (Manacor, Mallorca). Papers de la Societat Espeleològica Balear, 4, pp. 75–87.
Fornós, J.J., Ginés, À., Ginés, J., Gràcia, F., Merino, A., 2019. Littoral Endokarst from Mallorca Island (Western Mediterranean). In: The Spanish Coastal Systems. Springer, Cham, pp. 143–166.
Fornós, Joan J., Gelabert, Bernadí, 2011. Condicionants litològics i estructurals del carst a les illes Balears. Endins: publicació d'espeleologia, pp. 37–52.
Frost, C.D., Toner, R.N., 2004. Strontium isotopic identification of water-rock interaction and ground water mixing. Groundwwater 42, 418–432 (CrossRef).
Ghasemizadeh, R., Hellweger, F., Butscher, C., Padilla, I., Vesper, D., Field, M., Alshawabkeh, A., 2012. Groundwater flow and transport modeling of karst aquifers, with particular reference to the North Coast Limestone aquifer system of Puerto Rico. Hydrogeol. J. 20 (8), 1441–1461.
Giménez, J., Fornós Astó, Joan J., Gelabert, B., 2002. Análisis de la fracturación de los materiales calcáreos neógenos de la costa sudoriental de Mallorca.
Giménez, J., Barón, A., Comas, M., González, C., Garau, J., Beidas, O., Nadal, F.X., 2014. Hidrogeologia de les Illes Balears: les masses d'aigua càrstiques, 36. Endins: publicació d'espeleologia, pp. 9–26.
Ginés, A., Ginés, J., Fornós, J.J., Bover, P., Gómez-Pujol, L., Gràcia, F., Vicens, D., 2012. An introduction to the Quaternary of Mallorca. In: Ginés, A., Ginés, J., Gómez-Pujol, L., Onac, B.P., Fornós, J.J. (Eds.), Mallorca: A Mediterranean Benchmark for Quaternary Studies. Mon. Soc. Hist. Nat. Balears, 18, pp. 13–53.
Ginés, Joaquín, Ginés, Angel, Fornós, Joan J., 2021. "LES INVESTIGACIONS SOBRE EL CARST I LES COVES DE MALLORCA: EVOLUCIÓ DELS CONEIXEMENTS I PERSPECTIVES ACTUALS." Monografies de la Societat d'Història Natural de les Balears, 34.
Goldscheider, N., 2015. Overview of methods applied in karst hydrogeology. In: Karst Aquifers—Characterization and Engineering. Springer, Cham, pp. 127–145.
Goldscheider, N., Chen, Z., Auler, A.S., Bakalowicz, M., Broda, S., Drew, D., Hartmann, J., Jiang, G., Moosdorf, N., Stevanovic, Z., Veni, G., 2020. Global distribution of carbonate rocks and karst water resources. Hydrogeol. J. 28 (5), 1661–1677. https://doi.org/10.1007/s10040-020-02139-5.
Gràcia, F., Clamor, B., Gamundí, P., Fornós, J.J., 2010. El sistema de cavitats Gleda-Camp des Pou (Manacor, Mallorca). Endins: publicació d'espeleologia, pp. 35–68.
Gràcia, F., Clamor, B., Gamundí, P., Fornós, J.J., 2011. Morfologies de corrosió de la zona de mescla a les cavitats subaquàtiques de la franja litoral del Llevant i Migjorn de Mallorca. Endins: publicació d'espeleologia, pp. 133–146.
Green, N.R., MacQuarrie, K.T.B., 2014. An evaluation of the relative importance of the effects of climate change and groundwater extraction on seawater intrusion in coastal aquifers in Atlantic Canada. Hydrogeol. J. 22, 609–623. https://doi.org/10.1007/s10040-013-1092-y.
Gulley, J.D., Martin, J.B., Moore, P.J., Brown, A., Spellman, P.D., Ezell, J., 2015. Heterogeneous distributions of $CO_2$ may be more important for dissolution and karstification in coastal eogenetic limestone than mixing dissolution. Earth Surf. Process. Landf. 40 (8), 1057–1071.
Guo, Q., Zhang, Y., Zhou, Z., Zhao, Y., 2020. Saltwater transport under the influence of sea-level rise in coastal multilayered aquifers. J. Coast. Res. 36 (5), 1040–1049.
Guo, Y., Wen, Z., Zhang, C., Jakada, H., 2021. Contamination characteristics of chlorinated hydrocarbons in a fractured karst aquifer using TMVOC and hydro-chemical techniques. Sci. Total Environ. 794, 148717.
Han, D., Post, V.E., Song, X., 2015. Groundwater salinization processes and reversibility of seawater intrusion in coastal carbonate aquifers. J. Hydrol. 531, 1067–1080.
He, Z., Ma, C., Zhou, A., Qi, H., Liu, C., Cai, H., Zhu, H., 2018. Using hydrochemical and stable isotopic (δ2H, δ18O, δ11B, and δ37Cl) data to understand groundwater evolution in an unconsolidated aquifer system in the southern coastal area of Laizhou Bay, China. Appl. Geochem. 90, 129–141.
Homar, V., Ramis, C., Romero, R., Alonso, S., 2010. Recent trends in temperature and precipitation over the Balearic Islands (Spain). Clim. Chang. 98 (1), 199–211.
Jørgensen, N.O., Andersen, M.S., Engesgaard, P., 2008. Investigation of a dynamic seawater intrusion event using strontium isotopes (87Sr/86Sr). J. Hydrol. 348 (3–4), 257–269.
Kalhor, K., Ghasemizadeh, R., Rajic, L., Alshawabkeh, A., 2019. Assessment of groundwater quality and remediation in karst aquifers: a review. Groundw. Sustain. Dev. 8, 104–121.
Ketabchi, H., Mahmoodzadeh, D., Ataie-Ashtiani, B., Simmons, C.T., 2016. Sea-level rise impacts on seawater intrusion in coastal aquifers: review and integration. J. Hydrol. 535, 235–255.
Kresic, N., Panday, S., 2021. Modeling of groundwater flow and transport in coastal karst aquifers. Hydrogeol. J. 29 (1), 249–258.
Langman, J.B., Ellis, A.S., 2010. A multi-isotope (δD, δ18O, 87Sr/86Sr, and δ11B) approach for identifying saltwater intrusion and resolving groundwater evolution along the Western Caprock Escarpment of the Southern High Plains, New Mexico. Appl. Geochem. 25 (1), 159–174.
Li, C., Xing, L., Dong, Y., Peng, Y., Xing, X., Li, C., Zhao, Z., 2022. Numerical simulation and protection of the dynamic change of Jinan karst spring based on coupling of seepage and conduit flow. Heliyon 8 (9), e10428.
Li, Z., Yang, Q., Yang, Y., Ma, H., Wang, H., Luo, J., Martin, J.D., 2019. Isotopic and geochemical interpretation of groundwater under the influences of anthropogenic activities. J. Hydrol. 576, 685–697.

Lim, J.W., Lee, E., Moon, H.S., Lee, K.K., 2013. Integrated investigation of seawater intrusion around oil storage caverns in a coastal fractured aquifer using hydrogeochemical and isotopic data. J. Hydrol. 486, 202–210.
Long, Andrew J., Mahler, B.J., 2013. Prediction, time variance, and classification of hydraulic response to recharge in two karst aquifers. Hydrol. Earth Syst. Sci. 17 (1), 281–294.
López-García, J.M., Mateos Ruiz, R.M., 2003. La intrusión marina en los acuíferos de la isla de Mallorca. Tecnología de la Intrusión de Agua de Mar en Acuíferos costeros: Países Mediterráneos, 1. Instituto Geológico y Minero de España, pp. 383–392.
Lukač Reberski, J., Rubinić, J., Terzić, J., Radišić, M., 2020. Climate change impacts on groundwater resources in the coastal Karstic Adriatic area: a case study from the Dinaric Karst. Nat. Resour. Res. 29, 1975–1988.
Mahlknecht, J., Merchán, D., Rosner, M., Meixner, A., Ledesma-Ruiz, R., 2017. Assessing seawater intrusion in an arid coastal aquifer under high anthropogenic influence using major constituents, Sr and B isotopes in groundwater. Sci. Total Environ. 587, 282–295.
Maloszewski, P., Zuber, A., 1996. Lumped Parameter Models for the Interpretation of Environmental Tracer Data.
Mao, C., Tan, H., Song, Y., Rao, W., 2020. Evolution of groundwater chemistry in coastal aquifers of the Jiangsu, east China: insights from a multi-isotope (δ2H, δ18O, 87Sr/86Sr, and δ11B) approach. J. Contam. Hydrol. 235, 103730.
Marín, A.I., Francisco, M.R.J., Barberá, J.A., Fernández-Ortega, J., Matías, M., Damián, S., Bartolomé, A., 2021. Groundwater vulnerability to pollution in karst aquifers, considering key challenges and considerations: application to the Ubrique springs in southern Spain. Hydrogeol. J. 29 (1), 379–396.
Martin, J.B., Screaton, E.J., 2001. Exchange of matrix and conduit water with examples from the Floridan aquifer. In: US Geological Survey Karst Interest Group Proceedings. St Petersburg, Florida, pp. 38–44.
Martin, J.B., Gulley, J., Spellman, P., 2012. Tidal pumping of water between Bahamian blue holes, aquifers and the ocean. J. Hydrol. 416, 28–38.
Martin, J.M., Screaton, E.J., Martin, J.B., 2006. Monitoring well responses to karst conduit head fluctuations: implications for fluid exchange and matrix transmissivity in the Floridan aquifer. Geol. Soc. Am. Spec. Pap. 404, 209–217.
Masciopinto, C., Passarella, G., Caputo, M.C., Masciale, R., De Carlo, L., 2021. Hydrogeological models of water flow and pollutant transport in karstic and fractured reservoirs. Water Resour. Res. 57 (8), e2021WR029969.
Menning, D.M., Wynn, J.G., Garey, J.R., 2015. Karst estuaries are governed by interactions between inland hydrological conditions and sea level. J. Hydrol. 527, 718–733.
Mohammadi, Z., Illman, W.A., Field, M., 2021. Review of laboratory scale models of karst aquifers: approaches, similitude, and requirements. Groundwater 59 (2), 163–174.
Mongelli, G., Monni, S., Oggiano, G., Paternoster, M., Sinisi, R., 2013. Tracing groundwater salinization processes in coastal aquifers: a hydrogeochemical and isotopic approach in the Na-Cl brackish waters of northwestern Sardinia, Italy. Hydrol. Earth Syst. Sci. 17 (7), 2917–2928.
Mook, W.G. (Ed.), 2002. Isótopos ambientales en el ciclo hidrológico, Vol. 1. IGME.
Moragues, L., Ruano, P., Azañón, J.M., Garrido, C.J., Hidas, K., Booth Rea, G., 2021. Two Cenozoic extensional phases in Mallorca and their bearing on the geodynamic evolution of the Western Mediterranean. Tectonics 40 (11), e2021TC006868.
Motevalli, A., Moradi, H.R., Javadi, S., 2018. A comprehensive evaluation of groundwater vulnerability to saltwater up-coning and sea water intrusion in a coastal aquifer (case study: Ghaemshahr-juybar aquifer). J. Hydrol. 557, 753–773.
Nair, I.S., Brindha, K., Elango, L., 2021. Assessing the origin and processes controlling groundwater salinization in coastal aquifers through integrated hydrochemical, isotopic and hydrogeochemical modelling techniques. Hydrol. Sci. J. 66 (1), 152–164.
Neven, K., Sorab, P., 2021. Modeling of groundwater flow and transport in coastal karst aquifers. Hydrogeol. J. 29 (1), 249–258.
Nicault, Antoine, et al., 2008. Mediterranean drought fluctuation during the last 500 years based on tree-ring data. Clim. Dyn. 31, 227–245.
Panthi, J., Pradhanang, S.M., Nolte, A., Boving, T.B., 2022. Saltwater intrusion into coastal aquifers in the contiguous United States—a systematic review of investigation approaches and monitoring networks. Sci. Total Environ. 155641.
Puigserver, D., Herrero, J., Torres, M., Cortés, A., Nijenhuis, I., Kuntze, K., Carmona, J. M., 2016. Reductive dechlorination in recalcitrant sources of chloroethenes in the transition zone between aquifers and aquitards. Environ. Sci. Pollut. Res. 23, 18724–18741.
Puigserver, D., Carmona, J.M., Cortés, A., Viladevall, M., Nieto, J.M., Grifoll, M., Parker, B.L., 2013. Subsoil heterogeneities controlling porewater contaminant mass and microbial diversity at a site with a complex pollution history. J. Contam. Hydrol. 144 (1), 1–19.
Puigserver, D., Herrero, J., Nogueras, X., Cortés, A., Parker, B.L., Playà, E., Carmona, J. M., 2022. Biotic and abiotic reductive dechlorination of chloroethenes in aquitards. Sci. Total Environ. 816, 151532.
Purnama, S., Marfai, M.A., 2012. Saline water intrusion toward groundwater: issues and its control. J. Nat. Resour. Dev. 2, 25–32.
Reimann, T., Geyer, T., Shoemaker, W.B., Liedl, R., Sauter, M., 2011. Effects of dynamically variable saturation and matrix-conduit coupling of flow in karst aquifers. Water Resour. Res. 47 (11).
Ribeiro, S., Azevedo, M.R., Santos, J.F., Medina, J., Costa Sr., A., 2014. Isotopic signatures of Portuguese bottled mineral waters and their relationships with the geological setting. Comun. Geol. 101, 29–37.
Romanazzi, A., Gentile, F., Polemio, M., 2015. Modelling and management of a Mediterranean karstic coastal aquifer under the effects of seawater intrusion and climate change. Environ. Earth Sci. 74, 115–128.
Russak, A., Sivan, O., Yechieli, Y., 2016. Trace elements (Li, B, Mn and Ba) as sensitive indicators for salinization and freshening events in coastal aquifers. Chem. Geol. 441, 35–46.
Sàbat, F., Gelabert, B., Rodríguez-Perea, A., Giménez, J., Sàbat, F., et al., 2011. Geological structure and evolution of Majorca: implications for the origin of the Western Mediterranean. Tectonophysics 510 (1–2), 217–238.
Sappa, G., Vitale, S., Ferranti, F., 2018. Identifying karst aquifer recharge areas using environmental isotopes: a case study in Central Italy. Geosciences 8 (9), 351.
Shi, W., Lu, C., Werner, A.D., 2020. Assessment of the impact of sea-level rise on seawater intrusion in sloping confined coastal aquifers. J. Hydrol. 586, 124872.
Sivelle, V., Labat, D., Mazzilli, N., Massei, N., Jourde, H., 2019. Dynamics of the flow exchanges between matrix and conduits in karstified watersheds at multiple temporal scales. Water 11 (3), 569.
Smart, C.C., Worthington, S.R.H., 2004. Karst water resources. In: Gunn, J. (Ed.), Encyclopedia of Caves and Karst Science. Fitzroy Dearborn, New York, pp. 481–483.
Spivack, A.J., Edmond, J.M., 1987. Boron isotope exchange between seawater and the oceanic crust. Geochim. Cosmochim. Acta 51 (5), 1033–1043.
Srzić, V., Lovrinović, I., Racetin, I., Pletikosić, F., 2020. Hydrogeological characterization of coastal aquifer on the basis of observed sea level and groundwater level fluctuations: Neretva valley aquifer, Croatia. Water 12 (2), 348.
Stefánsson, A., Arnórsson, S., Sveinbjörnsdóttir, Á.E., Heinemaier, J., Kristmannsdóttir, H., 2019. Isotope (δD, δ18O, 3H, δ13C, 14C) and chemical (B, Cl) constrains on water origin, mixing, water-rock interaction and age of low-temperature geothermal water. Appl. Geochem. 108, 104380.
Stevanović, Z., 2019. Karst waters in potable water supply: a global scale overview. Environ. Earth Sci. 78 (23), 1–12.
Sun, Q., Gao, M., Wen, Z., Hou, G., Dang, X., Liu, S., Zhao, G., 2023. Hydrochemical evolution processes of multiple-water quality interfaces (fresh/saline water, saline water/brine) on muddy coast under pumping conditions. Sci. Total Environ. 857, 159297.
Surinaidu, L., Gupta, P.K., Ahmed, S., Hussain, M., Nandan, M.J., 2023. Impact of urban wastewater reuse for irrigation on hydro-agro-ecological systems and human health risks: a case study from Musi river basin, South India. HydroResearch 6, 122–129.
Syafiuddin, A., Boopathy, R., Hadibarata, T., 2020. Challenges and solutions for sustainable groundwater usage: pollution control and integrated management. Curr. Pollut. Rep. 6, 310–327.
Teotónio, C., Rodríguez, M., Roebeling, P., Fortes, P., 2020. Water competition through the ‘water-energy’ nexus: assessing the economic impacts of climate change in a Mediterranean context. Energy Econ. 85, 104539.
USDA, 2012. U.S. Department of Agriculture. National Soil Survey Handbook, Title 430-VI. (Available online). 12, 2012. Natural Resources Conservation Service, pp. 1–19.
Vallejos, A., Díaz-Puga, M.A., Sola, F., Daniele, L., Pulido-Bosch, A., 2015. Using ion and, isotope characterization to delimitate a hydrogeological macrosystem. Sierra de Gádor (SE, Spain). J. Geochem. Explor. 155, 14–25.
Vera, I., Mariño-Tapia, I., Enriquez, C., 2012. Effects of drought and subtidal sea-level variability on salt intrusion in a coastal karst aquifer. Mar. Freshw. Res. 63 (6), 485–493.
Wang, H., Ni, J., Song, Q., Li, C., Wang, F., Cao, Y., 2021. Analysis of coastal groundwater hydrochemistry evolution based on groundwater flow system division. J. Hydrol. 601, 126631.
Wang, X., 2010. On the coupled continuum pipe flow model (CCPF) for flows in karst aquifer. Discrete Continuous Dyn. Syst. B 13 (2), 489.
Wang, Y., Guo, Q., Su, C., Ma, T., 2006. Strontium isotope characterization and major ion geochemistry of karst water flow, Shentou, northern China. J. Hydrol. 328 (3–4), 592–603.
Werner, A.D., Bakker, M., Post, V.E., Vandenbohede, A., Lu, C., Ataie-Ashtiani, B., Barry, D.A., 2013. Seawater intrusion processes, investigation and management: recent advances and future challenges. Adv. Water Resour. 51, 3–26.
White, W.B., 2016. Groundwater flow in karstic aquifers. In: The Handbook of Groundwater Engineering. CRC Press, pp. 581–614.
White, W.B., Herman, E., Rutigliano, M., Herman, J., Vesper, D., Engel, S., 2016. Karst groundwater contamination and public health. In: Leesburg VA Karst Waters Inst. Spec. Publ, 19, pp. 1–347.
Wöppelmann, Guy, Marcos, Marta, 2012. Coastal sea level rise in southern Europe and the nonclimate contribution of vertical land motion. J. Geophys. Res. Oceans 117, C1.
Wu, X., Xu, Z., Xu, Z., Hu, B.X., Chang, Q., Hu, Y., 2022. The influence of seasonal recharge and groundwater pumping on the seawater intrusion in a coastal karst aquifer. J. Coast. Res. 38 (4), 785–794.
Wu, Y., Hunkeler, D., 2017. Sedimentary roles on hyporheic exchange in karst conduits at low Reynolds numbers by laboratory experiments. Hydrogeol. J. 25 (3), 787–798. https://doi.org/10.1007/s10040-016-1531-7.
Xu, Z., Bassett, S.W., Hu, B., Dyer, S.B., 2016. Long distance seawater intrusion through a karst conduit network in the Woodville Karst Plain, Florida. Sci. Rep. 6, 32235 https://doi.org/10.1038/srep32235.
Xu, Z., Hu, B.X., Ye, M., 2018. Numerical modeling and sensitivity analysis of seawater intrusion in a dual-permeability coastal karst aquifer with conduit networks. Hydrol. Earth Syst. Sci. 22 (1), 221–239.
Xu, Z., Hu, B.X., Xu, Z., Wu, X., 2019. Simulating seawater intrusion in a complex coastal karst aquifer using an improved variabledensity fow and solute transport–conduit fow process model. Hydrogeol. J. 27, 1277–1289. https://doi.org/10.1007/s10040-018-1903-2.
Yadav, M.P., Agarwal, R., Purohit, S.D., Kumar, D., Suthar, D.L., 2022. Groundwater flow in karstic aquifer: analytic solution of dual-porosity fractional model to simulate groundwater flow. Appl. Math. Sci. Eng. 30 (1), 598–608.

Zamrsky, Daniel, et al., 2020. Geological heterogeneity of coastal unconsolidated groundwater systems worldwide and its influence on offshore fresh groundwater occurrence. Front. Earth Sci. 7, 339.
Zhang, C., Li, X., Ma, J., Wang, Z., Hou, X., Gao, M., Zuo, X., 2022a. Combining stable isotope (2H, $^{18}O$ and $^{87}Sr/^{86}Sr$) and hydrochemistry to understand hydrogeochemical processes in karst groundwater system, Xin'an, northern China.
Zhang, Y., Svyatsky, D., Rowland, J.C., Moulton, J.D., Cao, Z., Wolfram, P.J., Pasqualini, D., 2022b. Impact of coastal marsh eco-geomorphologic change on saltwater intrusion under future sea level rise. Water Resour. Res. e2021WR030333.
Zhao, L.J., Yang, Y., Cao, J.W., Wang, Z., Luan, S., Xia, R.Y., 2022. Applying a modified conduit flow process to understand conduit-matrix exchange of a karst aquifer. China Geol. 5 (1), 26–33.